



Advanced Photon Source Upgrade

Advanced Photon Source Upgrade Project

**SynRad and MolFlow+ Analysis of the APS-U Storage Ring
Vacuum System for the 41pm V5.1 lattice**

Draft

[July 27, 2017]

Document Number: _____
ICMS Content ID: **APSU_1688669**

Version Control

This printed or electronic version of the document may not be the current or approved revision. The current revision is maintained in the Advanced Photon Source Upgrade (APS-U) Project's Integrated Content Management System (ICMS) where all internal Project document approvals are managed. ICMS can be accessed through the web by authorized users, <https://icmsdocs.aps.anl.gov/>, and this document can be identified by the document and version number as indicated in the Version Control Table below. Note that the version number in the table below and in ICMS may not match. The current approved version is always available in ICMS. Contact the Responsible Person listed below if you are not able to locate the controlled version or access ICMS.

DOCUMENT No.	WBS No.	REVISION No.	ICMS CONTENT ID
	U.2.2.1.1.4	0	APSU_1688669

Approvals for this document will be required from:

Jason Carter – Author, Mechanical Engineer AES-MED Group

Ben Stillwell – APS-U Storage Ring Vacuum System Design Group Leader
Mechanical Engineer, AES-MED Group

Version Control Log

Document Number	Revision	Responsible Person	Version Date	Description of Change

Table of Contents

Version Control.....	ii
Table of Contents	iii
List of Figures.....	v
List of Tables	viii
Acronyms and Abbreviations	viii
1. Introduction: Vacuum simulations in SynRad and MolFlow+.....	1
2. Model geometry for SynRad and MolFlow+	1
2.1. 3D model of MBA vacuum system.....	1
2.2. SynRad ray trace verification.....	5
3. Pumping in MolFlow+	8
3.1. Discrete pump pumping speeds	8
3.1.1. TiTan 45S-DI ion pump.....	10
3.1.2. CapaciTorr D200.....	12
3.1.3. Total discrete pump speeds	13
3.2. NEG strips pumping speeds.....	14
3.3. NEG coating pumping speeds.....	18
4. Photon stimulated desorption in MolFlow+	20
4.1. Notes about PSD yield experiments.....	20
4.2. Importing PSD outgassing into MolFlow+	22
4.2.1. Aluminum outgassing map	27
4.2.2. OFHC copper outgassing map	31
4.2.3. Cu-plated stainless steel outgassing map	33
4.2.4. NEG coated stainless steel outgassing map	34
5. SynRad simulation and results	36
5.1. SynRad model assumptions	36
5.1.1. Photon reflectivity in SynRad.....	36

5.2.	SynRad Results	38
5.3.	Comments on results.....	39
6.	MolFlow+ simulation and results	39
6.1.	PSD outgassing import	40
6.2.	MolFlow+ results	41
6.2.1.	NEG saturation/failure analysis	45
6.3.	Comments on results.....	46
6.3.1.	Comments on aluminum PSD measurement study	47
References.....		48

List of Figures

Figure 2.1.1: Creo assembly of one sector of the MBA storage ring.....	2
Figure 2.1.2: Single part CAD representation of one sector of the 41pm V5.1 MBA storage ring.....	3
Figure 2.1.3: Inline absorbers in the SynRad/MolFlow+ geometry highlighted in red	4
Figure 2.2.1 Example section of 2D ray trace.....	6
Figure 2.2.2 SynRad model ray trace, photon distribution in green	7
Figure 3.1.1 Pumping facets in a MBA storage ring sector MolFlow+ model highlighted in red.....	9
Figure 3.1.2 Discrete pump surface area highlighted in red for a MolFlow+ simulation of the APS-U MBA SR vacuum system.....	10
Figure 3.1.3 Titan 45S Ion Pump pumping speed vs pressure.....	11
Figure 3.1.4 Differential ion pump performance from Perkin-Elmer instruction manual	12
Figure 3.1.5 SAES CapaciTorr D200 pumping speed vs sorbed quantity	13
Figure 3.2.1 Pumping speed vs Sorbed Quantity for SAES Getters ST 707/ CTAM/ 30D Strip (Digitized curves in orange and blue)	14
Figure 3.2.2 ST707 Pumping Speed vs Sorbed Quantity.....	15
Figure 3.2.3 ST707 Pumping Speed vs APS-U MBA	16
Figure 3.2.4 NEG strip surface area highlighted in red for a MolFlow+ simulation of the APS-U MBA SR vacuum system.....	17
Figure 3.3.1 Ti-Zr-V pumping speed vs CO surface coverage	18
Figure 3.3.2 NEG coated surface area highlighted in red for a MolFlow+ simulation of the APS-U MBA SR vacuum system, ~2940 cm ² approximate surface area of chambers	19
Figure 4.1.1 PSD yield experimental setup at the U10B beamline at NSLS	20
Figure 4.1.2 PSD yield experimental setup at the X28A beamline at NSLS	21
Figure 4.1.3 PSD yield experimental setup at the D31 beamline at ESRF.....	21
Figure 4.2.1 Example log scale flux density rate (photons/second/cm ²) map computed for a SynRad simulation with photon scattering	23
Figure 4.2.2 MolFlow+ (v 2.5.6) menu for translating a SynRad flux map into PSD outgassing.....	24
Figure 4.2.3 Typical ray trace for design of a laboratory PSD measurement.....	24

Figure 4.2.4 Ray trace from a PSD measurement recreated in SynRad with photon scattering	25
Figure 4.2.5 SynRad photon flux densities computed for the recreation of a typical PSD measurement ..	26
Figure 4.2.6 Diagram of iterative process for calibrating PSD yields for use in MolFlow+ where the approximated PSD functions are used to map the fluxes from Figure 4.2.18 to outgassing in MolFlow+. The functions are adjusted until the predicted outgassing matches the original data	26
Figure 4.2.7 Comparison of three of the four aluminum chamber cross sections with published PSD measurements.....	27
Figure 4.2.8 Mathewson PSD measurement from an elliptical aluminum chamber.....	28
Figure 4.2.9 Kobari PSD measurement from an aluminum NSLS extrusion	28
Figure 4.2.10 Grobner PSD measurement from an aluminum LEP extrusion.....	29
Figure 4.2.11 Foerster PSD measurement from an aluminum APS extrusion.....	29
Figure 4.2.12 CAD models of the four chamber geometries for use in MolFlow+	30
Figure 4.2.13 Four aluminum PSD measurements recreated in SynRad with photon flux densities (photons/cm ² /s) in log scale	30
Figure 4.2.14 Comparison of four published H ₂ PSD yields measured on various aluminum chambers...	31
Figure 4.2.15 Copper chamber PSD measurement experiment recreated in SynRad.....	32
Figure 4.2.16 PSD measurement from an OFHC copper PEP-II style vacuum chamber	32
Figure 4.2.17 Cu-plated stainless steel PSD measurement experiment recreated in SynRad without photon scattering	33
Figure 4.2.18 PSD yield vs accumulated photons for a copper plated stainless steel vacuum chamber	34
Figure 4.2.19 NEG coated stainless steel PSD measurement experiment recreated in SynRad without photon scattering	35
Figure 4.2.20 PSD yield vs accumulated photons for a NEG coated stainless steel vacuum chamber	35
Figure 5.1.1 Aluminum surface reflectivity in SynRad	37
Figure 5.1.2 Copper surface reflectivity in SynRad.....	37
Figure 5.2.1 SynRad steady state flux density rate distribution in photons/s/cm ² (log scale over 8 orders of magnitude)	38
Figure 6.1.1: Aluminum surfaces for PSD import	40
Figure 6.1.2 Oxygen free copper (OFHC) surfaces for PSD import	40
Figure 6.1.3 NEG coated surfaces for PSD import.....	41
Figure 6.2.1 Gas specific MolFlow+ pressure profiles @ 100 A*hrs. beam conditioning for a simulation using the Kobari (NSLS) aluminum PSD measurment.....	42
Figure 6.2.2 Gas specific MolFlow+ pressure profiles @ 1000 A*hrs. beam conditioning for a simulation using the Kobari (NSLS) aluminum PSD measurment.....	43

Figure 6.2.3 Total pressure comparison @ 1000 A*hrs using four separate aluminum PSD measurements	44
Figure 6.2.4 Comparison of APS-U conditioning curves for four aluminum PSD measurements.....	45
Figure 6.2.5 Comparison of APS-U pressures for various NEG saturation or failure scenarios	46

List of Tables

Table 2.1.1: Locations of absorbers and their distance from the beam.....	5
Table 2.2.1: Total power loads at 200 mA beam current on photon absorbers from a SynRad ray trace	8
Table 3.1.1 Total discrete pump pumping speeds for use in MolFlow+ (@ 1000 A*hrs. or less beam conditioning).....	13
Table 3.2.1 L-Bend chamber NEG strip H ₂ sorption rate approximation.....	15
Table 3.2.2 L-Bend chamber NEG strip CO sorption rate approximation	16
Table 3.2.3 Pump speeds for MolFlow+ simulation for a 2.2m long NEG strip @ 1000 A*hrs. operating time	17
Table 3.3.1 NEG Coating sticking factors for MolFlow+ simulations	19
Table 6.1.1 Comparison of total outgassing @ 1000 A*hrs using four separate aluminum PSD measurements.....	41
Table 6.2.1 Comparison of total pressure @ 1000 A*hrs conditioning using four separate aluminum PSD measurements.....	44
Table 6.2.2 Comparison of average gas compositions @ 1000 A*hrs conditioning using four separate aluminum PSD measurements	44

Acronyms and Abbreviations

1. Introduction: Vacuum simulations in SynRad and MolFlow+

This report documents how the vacuum simulation package SynRad/MolFlow+ [1] is used to estimate the ultra-high vacuum (UHV) pressures for the APS-U MBA storage ring vacuum system for the lattice version ‘H7BA-TwoSector-nux95-nuy36-3PW-RB-41pm-Version5Rev1’ [2]. Dr. Roberto Kersevan and Dr. Marton Ady of CERN’s Vacuum Surfaces and Coating Technology Group wrote the two programs and provided close consultation of simulations for the MBA storage ring vacuum system.

MolFlow+ computes UHV pressures given pumping and outgassing definitions. SynRad computes photon flux distributions generated from magnetic sources. The two programs share 3D model geometry for coupled ray trace and vacuum system calculations. The coupled calculations use experimental data to convert SynRad photon flux distributions into dynamic photon stimulated desorption (PSD) outgassing in a MolFlow+ simulation. The inclusion of PSD outgassing allows for computations of dynamic vacuum pressures for estimation of beam lifetimes.

Section 2 details the creation of model geometry for both the SynRad and MolFlow+ models and how the SynRad generated photon distribution is verified to a 2D ray trace.

Section 3 lists the pumping speeds assumed for the discrete pumps, NEG strips, and NEG coated surfaces within the MBA vacuum system.

Section 4 shows how SynRad flux maps are translated to PSD outgassing. This includes comparisons of material specific experimental results and how they are used as maps to compute gas specific dynamic PSD outgassing in MolFlow+.

Section 5 details the assumptions and results for the SynRad simulation of the MBA storage ring vacuum system.

Section 6 details the assumptions and results for the MolFlow+ simulation of the MBA storage ring vacuum system.

2. Model geometry for SynRad and MolFlow+

Coupled SynRad/MolFlow+ vacuum simulations must share equal 3D geometry so a model is created that is suitable for the purposes of each program. Both programs require a model that represents the interior volume under vacuum. This leads to model geometry whose outer surfaces represent the interior chamber surfaces of the vacuum system. For SynRad, a model must accurately capture the ray trace and photon distribution with accurately located shielding features. For MolFlow+, the volumes and shapes of vacuum chamber interiors are accurately modeled to capture variations in pumping conductance.

2.1. 3D model of MBA vacuum system

A detailed model of the MBA vacuum system is created with the concept of ‘inverting’ a detailed 3D CAD model of a full sector of the MBA storage ring, see Figure 2.1.1, in order to capture the interior volume

under vacuum. A single part CAD model fills the empty vacuum space of the full model assembly, see Figure 2.1.2.

Both models feature chamber curvature that ties to points from the lattice file. Close coordination between the chamber curvature and the lattice file allows for an accurate SynRad ray trace within the narrow tube geometry that spans ~27 meters per sector. Planar cuts into the vacuum volume geometry reflect the intended photon shielding in the vacuum system.

Figure 2.1.3 shows the locations of photon absorbers in the vacuum system. A numerical method for off-orbit ray tracing calculated the optimized absorber heights. Table 2.1.1 details the locations of absorbers. The 'S distance' in Table 2.1.1 is the distance from the center of the preceding ID straight section as measured along the nominal particle beam trajectory.

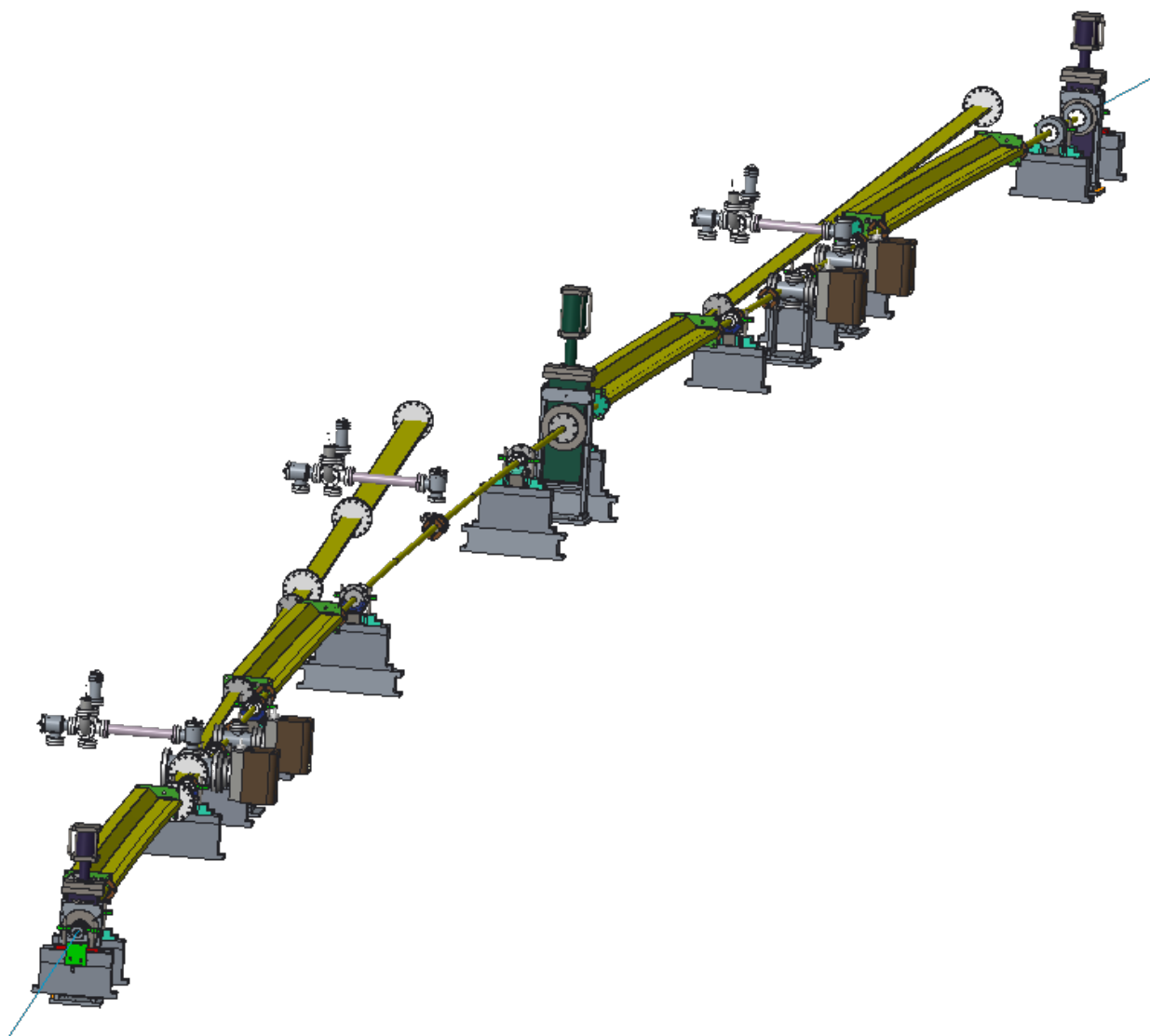


Figure 2.1.1: Creo assembly of one sector of the MBA storage ring

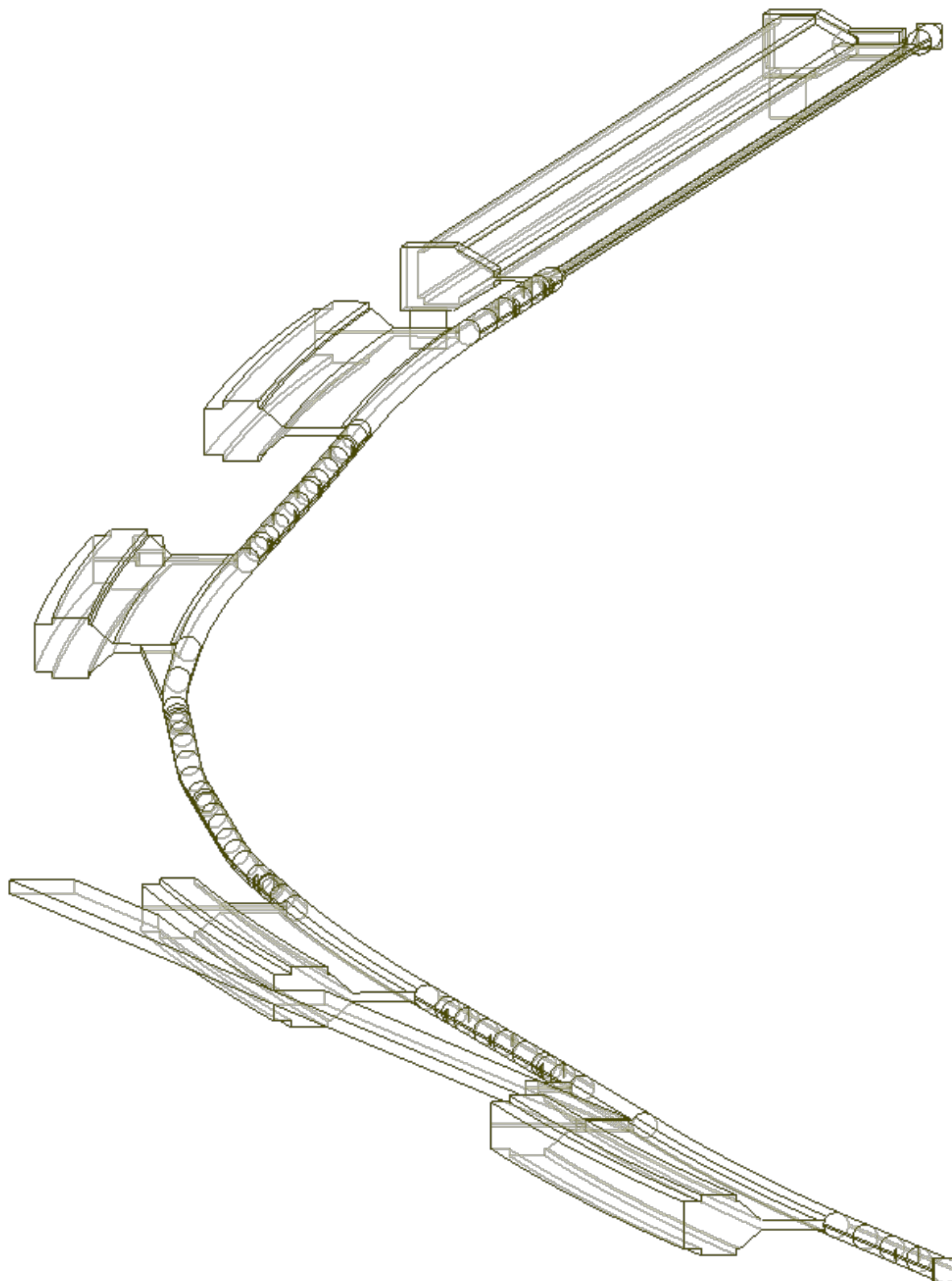


Figure 2.1.2: Single part CAD representation of one sector of the 41pm V5.1 MBA storage ring

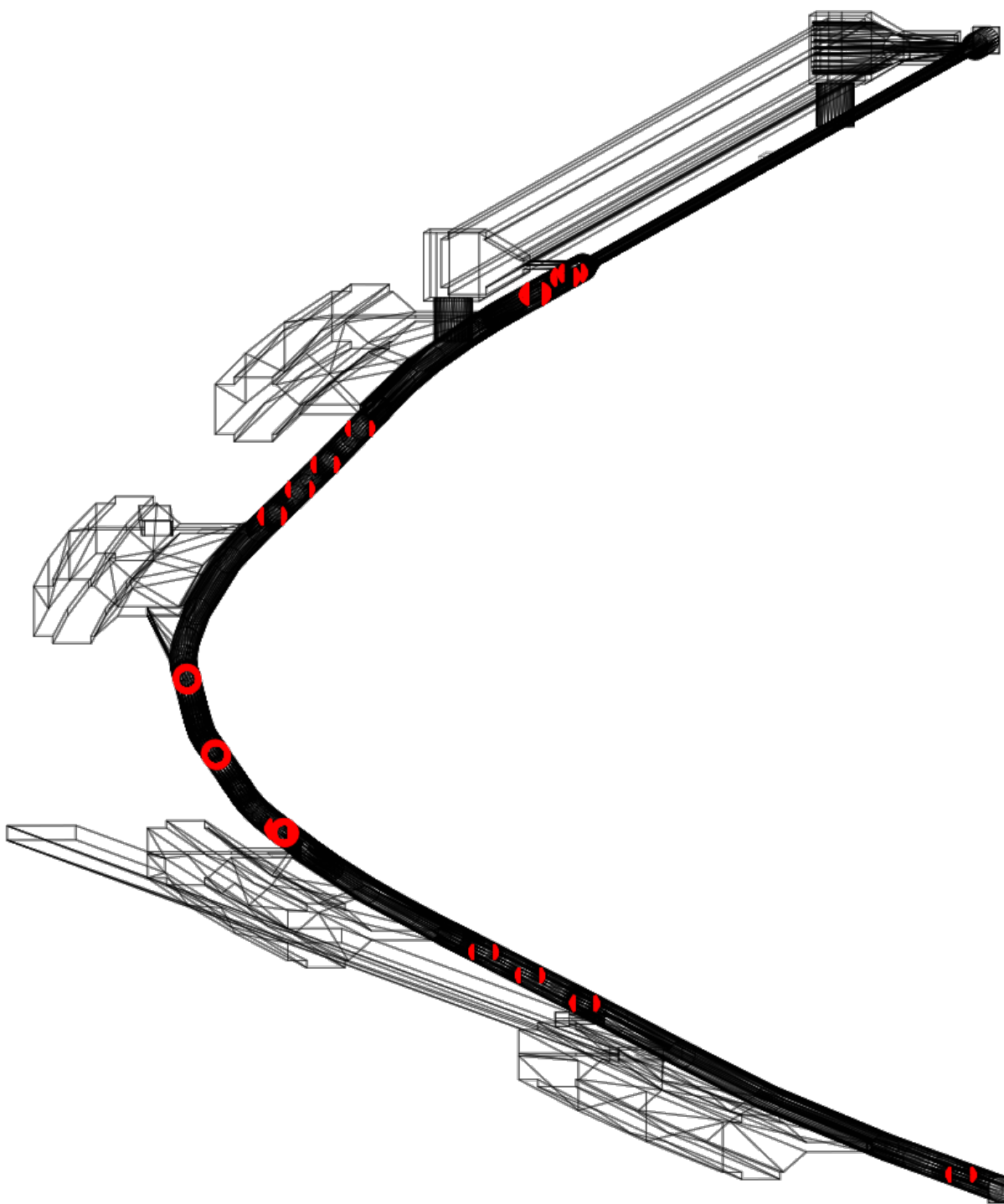


Figure 2.1.3: Inline absorbers in the SynRad/MolFlow+ geometry highlighted in red

ABSORBER	S COORD.	DISTANCE FROM ABSORBER TIP TO BEAM (METERS)	(MILLIMETERS)
A:VC1A	3.171	9.31	
A:CA1	6.904	8.87	
A:VC7A	7.286	8.94	
A:VC8A	7.954	9.29	
A:VC9A	8.520	9.23	
A:EA2	10.882	7.82	
A:VC12A	11.385	7.45	
A:P5A	11.470	7.49	
A:VC13A	13.255	8.17	
A:VC15A	15.064	8.00	
B:CA1	18.650	8.37	
B:VC8A	18.970	8.26	
B:VC7A	19.612	8.95	
B:VC6A	20.204	8.93	
B:VC5A	21.067	9.22	
B:EA1	23.730	7.49	
B:FA3	24.310	6.33	
B:FA2	24.675	8.37	
B:FA1	24.811	8.31	
STRAIGHT	30.176	8.94	

Table 2.1.1: Locations of absorbers and their distance from the beam

2.2. SynRad ray trace verification

The ray trace generated by SynRad compares closely to 2D CAD generated ray traces [3] [4], see Figure 2.2.1, Figure 2.2.2, and Table 2.2.1, usually within less than 1% for individual components such as photon absorbers. Table 2.2.1 lists the total power loads for individual photon absorbers at 200 mA beam current.

A symmetric boundary condition in SynRad passes photons from the downstream end of the model to the upstream and enables an accurate full sector ray trace. Figure 2.2.2 shows the symmetric boundary transfer where the pink dotted lines represent the ‘teleporting’ of photons from one boundary to the next.

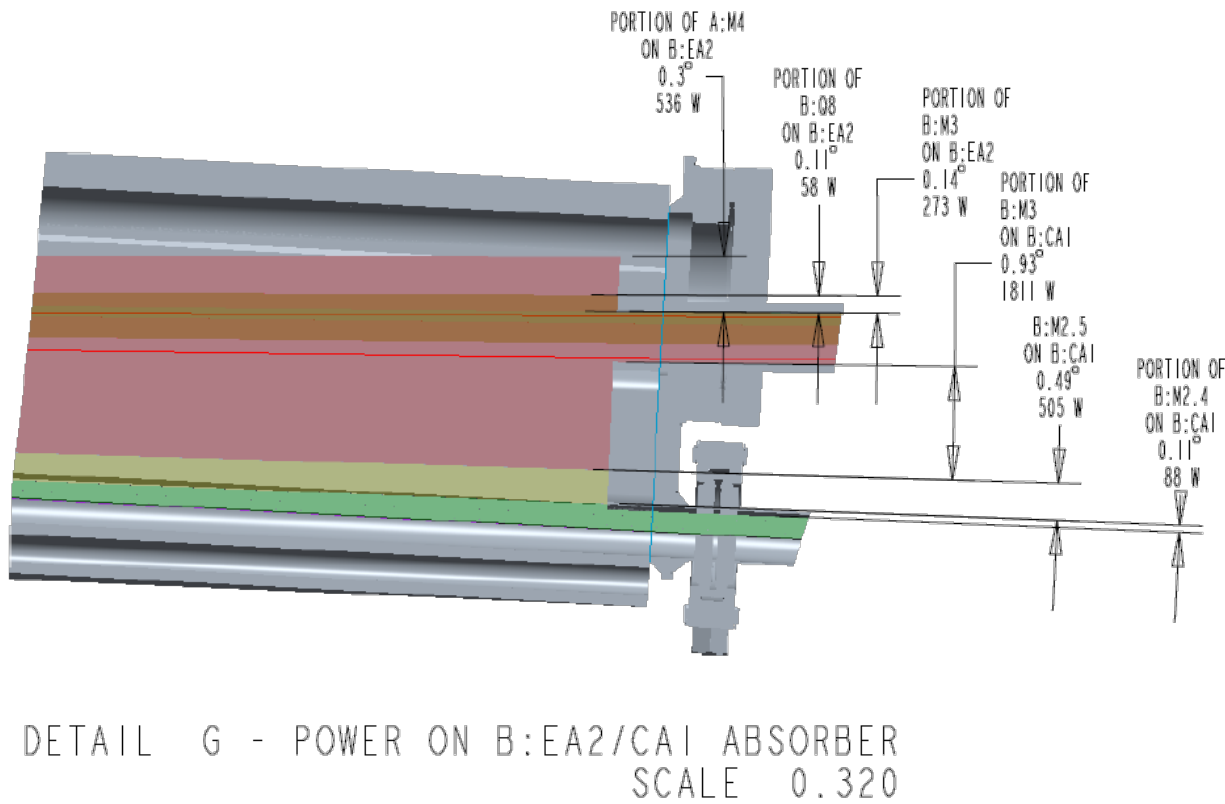


Figure 2.2.1 Example section of 2D ray trace

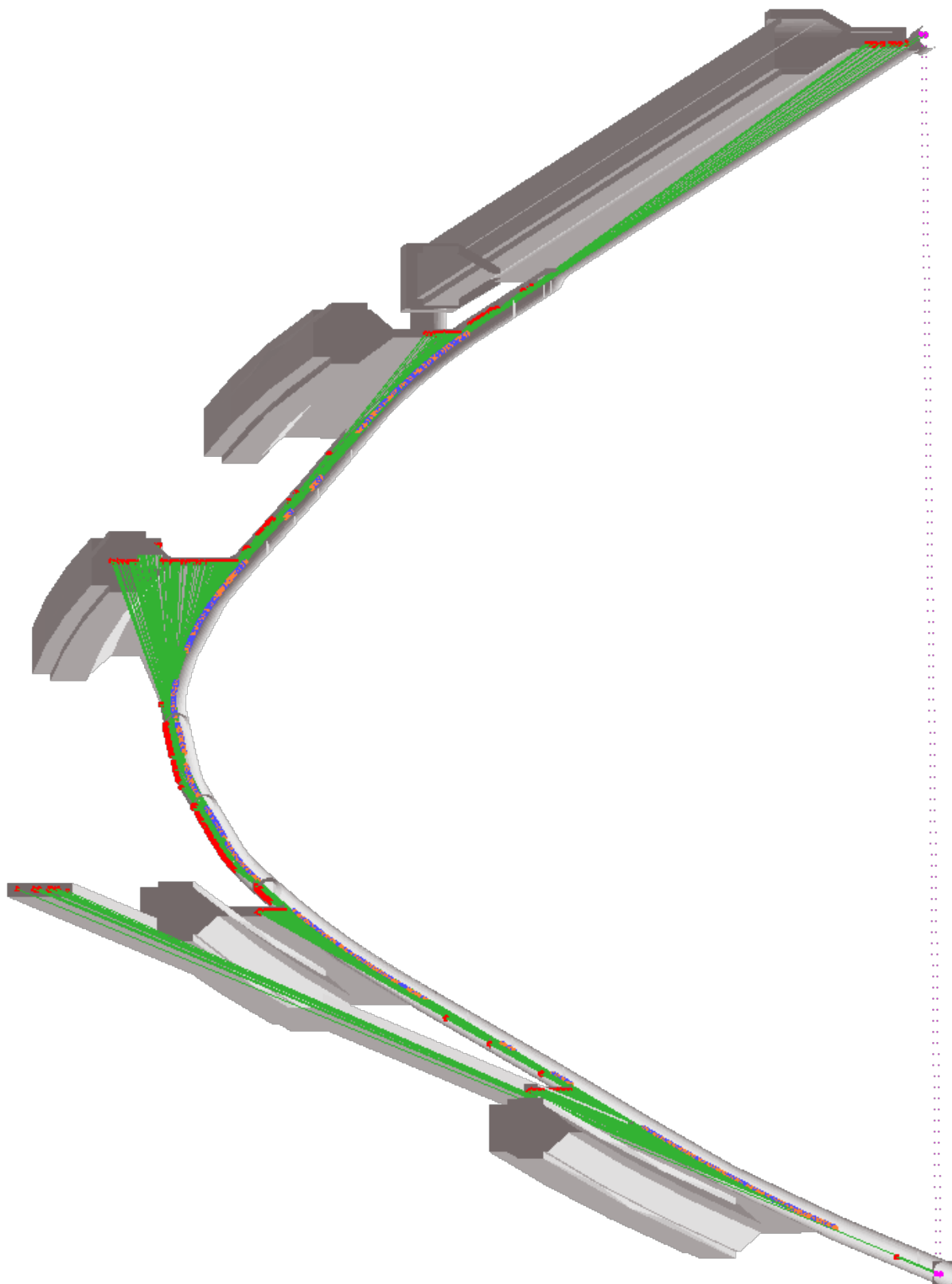


Figure 2.2.2 SynRad model ray trace, photon distribution in green

ABSORBER	SYNRAD (W)
A:VC1A	7
A:CA1	997
A:VC7A	36
A:VC8A	23
A:VC9A	17
A:EA2	458
A:VC12A	151
A:P5A	18
A:VC13A	283
A:VC15A	279
B:CA1	2434
B:VC8A	84
B:VC7A	46
B:VC6A	34
B:VC5A	20
B:EA1	528
B:FA3	280
B:FA2	97
B:FA1	46
STRAIGHT	644

Table 2.2.1: Total power loads at 200 mA beam current on photon absorbers from a SynRad ray trace

3. Pumping in MolFlow+

Figure 3.1.1 highlights where pumping is located in a MolFlow+ model of the MBA storage ring vacuum system. Pumping is applied as a bulk speed or sticking coefficient to surface elements called ‘facets’. NEG coating is applied as a sticking factor on the FODO section chambers. NEG strip pumping is provided in the antechambers of the L-bend and straight section chambers by long facets with equivalent surface area of a typical strip. Discrete pumps are in eleven locations including at end absorbers and crotch absorbers. Pumping cross geometry is not included the model in Figure 3.1.1 but the pumping speed from the discrete pumps can be scaled appropriately to factor in conductance limitations. One advantage of MolFlow+ is that the conductance of complex chambers are automatically included in the computation process.

3.1. Discrete pump pumping speeds

Discrete pumps will be provided in eleven locations per sector of the MBA storage ring vacuum system, see Figure 3.1.2. Each pump will include the combination of an ion pump and a NEG cartridge pump. Pumping speeds are first estimated for the two pumping elements based on manufacturing data and are summed to provide total pumping speed for use in MolFlow+ simulations. Finally, the pumping speeds are scaled to include the effect of conductance based on expected pumping cross geometry that is not included in this model.

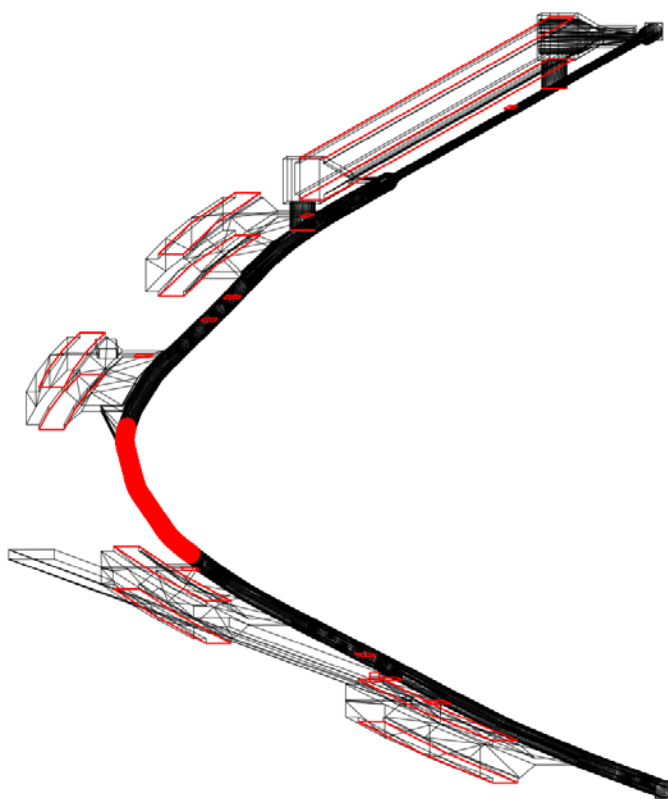


Figure 3.1.1 Pumping facets in a MBA storage ring sector MolFlow+ model highlighted in red

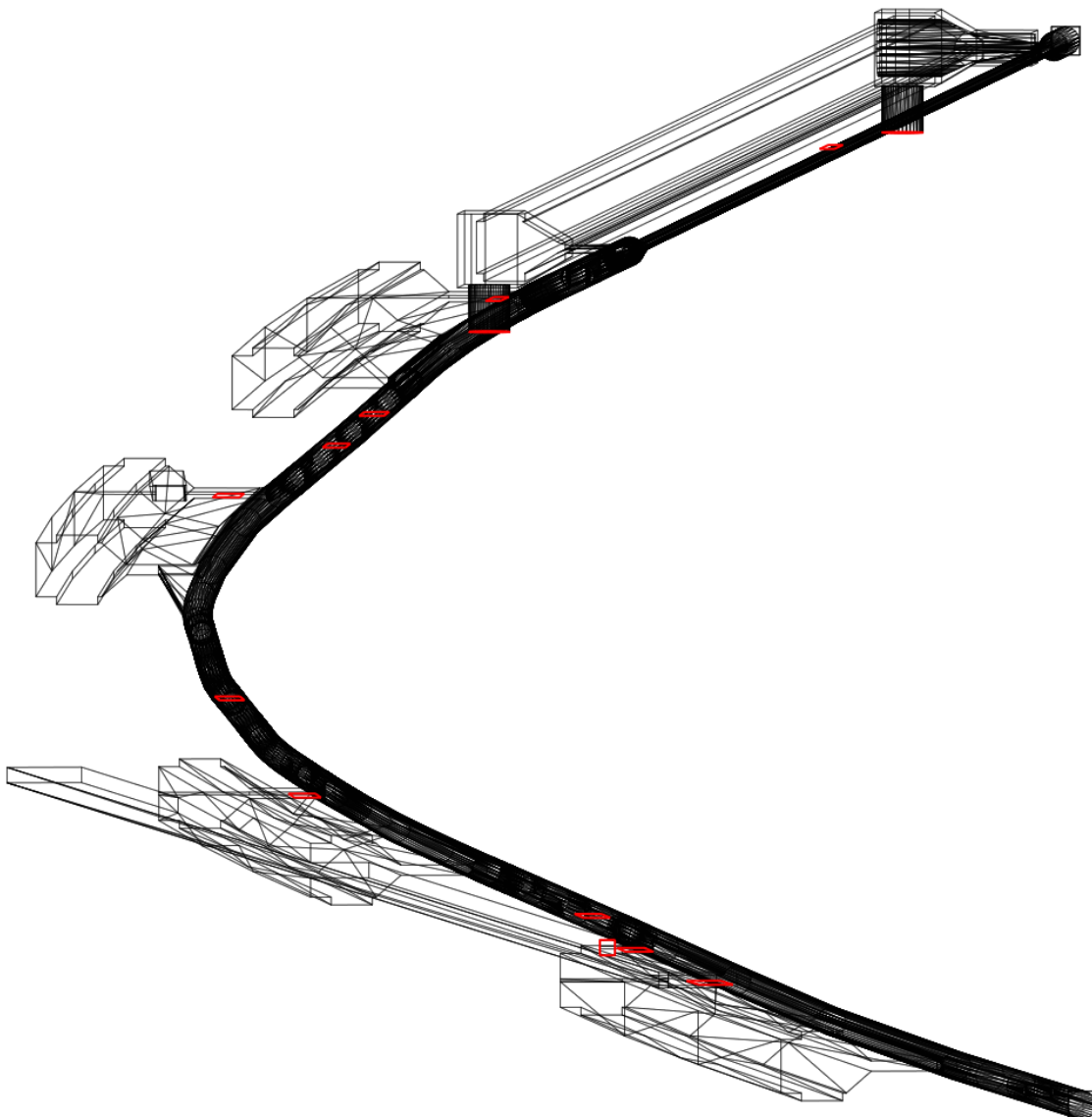


Figure 3.1.2 Discrete pump surface area highlighted in red for a MolFlow+ simulation of the APS-U MBA SR vacuum system

3.1.1. TiTan 45S-DI ion pump

The TiTan 45S ion pump [7] will be employed at each of eleven discrete pumping locations. Figure 3.1.3 is a plot provided by the manufacturer of the nitrogen pumping speed vs pump pressure. The system pressure at the ion pumps is assumed to be about 1E-9 mbar. Figure 3.1.3 shows the TiTan 45S-DI pump has a nitrogen equivalent pumping speed of 22 L/s at 1E-9 mbar. This nitrogen equivalent pumping speed then must be appropriately scaled to apply to the individual gas species of interest. The Perkin Elmer instruction manual for ion pumps [8] provides a table for converting pumping speeds per gas species based on a reference, see Figure 3.1.4. This table is used with the 22 L/s assumed reference speed to determine an ion pump speed for each gas. For example, the H₂ pump speed is equal to 22 L/s * (1.6 / 0.85) = 41.4 L/s.

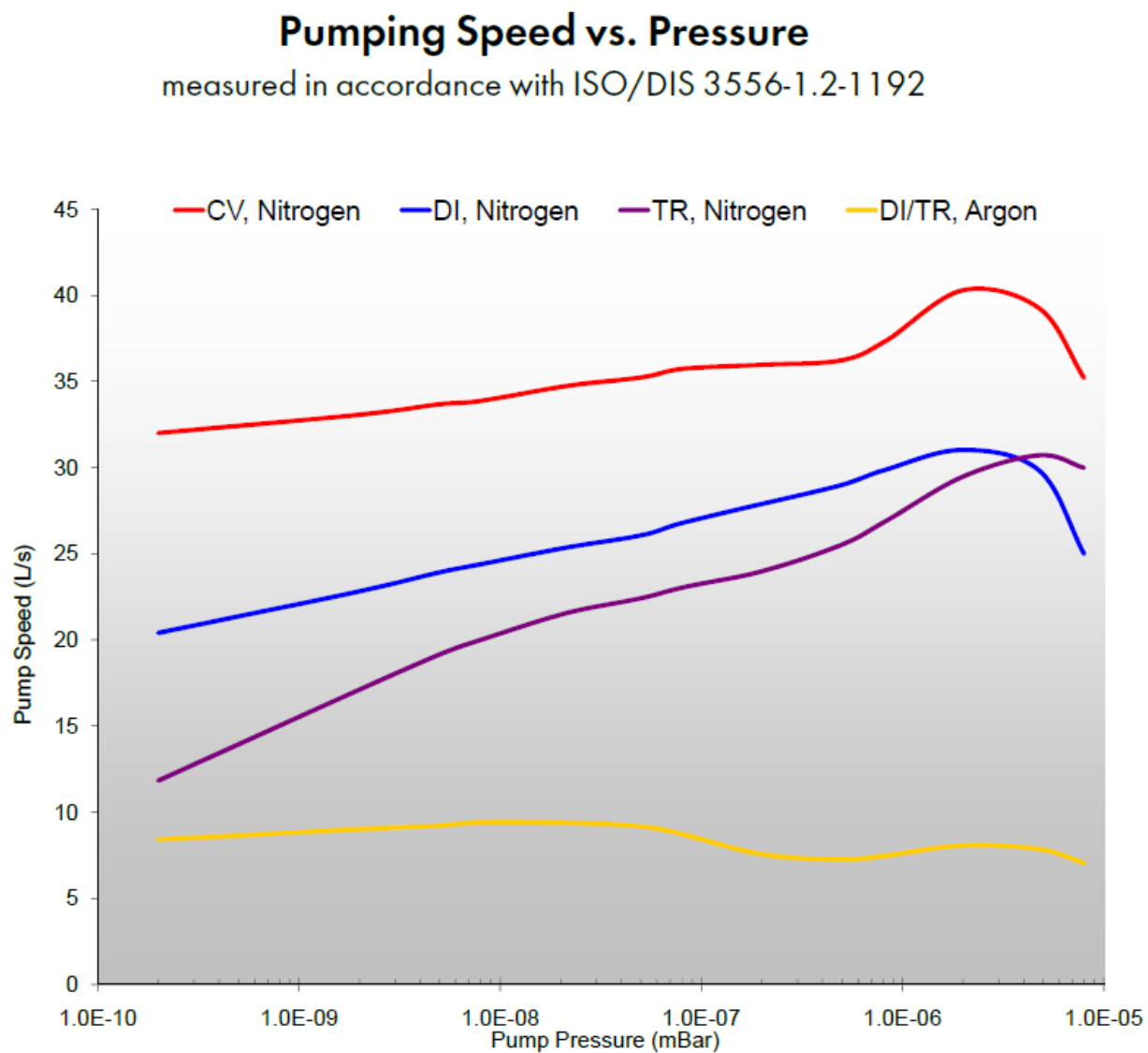


Figure 3.1.3 Titan 45S Ion Pump pumping speed vs pressure

TABLE 4
PUMPING SPEEDS (Percent of Rated Speed)
CONVENTIONAL ION PUMPS

Hydrogen	250%
Carbon Dioxide	100%
Nitrogen	85%
Oxygen	70%
Water Vapor	100%
Helium.....	10%
Argon	2%
Light Hydrocarbons	0%

DIFFERENTIAL ION PUMPS

Hydrogen	160%
Carbon Dioxide	100%
Nitrogen	85%
Oxygen	70%
Water Vapor	100%
Helium.....	30%
Argon	20%

Figure 3.1.4 Differential ion pump performance from Perkin-Elmer instruction manual

3.1.2. CapaciTorr D200

CapaciTorr D200 NEG cartridge pumps [9] will be employed at each of the eleven discrete pumps. Figure 3.1.5 shows that the H₂ pumping speed for the D200 is a near constant 200 L/s, regardless of sorbed quantity. NEG cartridge pumps are assumed to not pump CH₄.

CO has a peak pumping speed of 100 L/s which begins to decrease after a sorbed quantity of 1E-2 Torr*L is reached. For a conservative ‘beam on’ CO outgassing rate of 1E-12 Torr*L/s/cm² at 1000 @ A*hrs. (or 1.8E7 seconds for a 0.2 mA machine) the total sorbed gas would be 1.8E-5 Torr*L/cm². This high surface rate would have to be distributed across ~1E3 cm² to reach the pump speed reduction point @ 1000 A*hrs. It is assumed that this will be far from the case as the high outgassing will come from local beam foot prints so the pump speed @ 1000 A*hrs. is assumed to be a constant 100 L/s.

Data is not provided for the gases CO₂ and H₂O so it is assumed that they will behave similarly to CO.

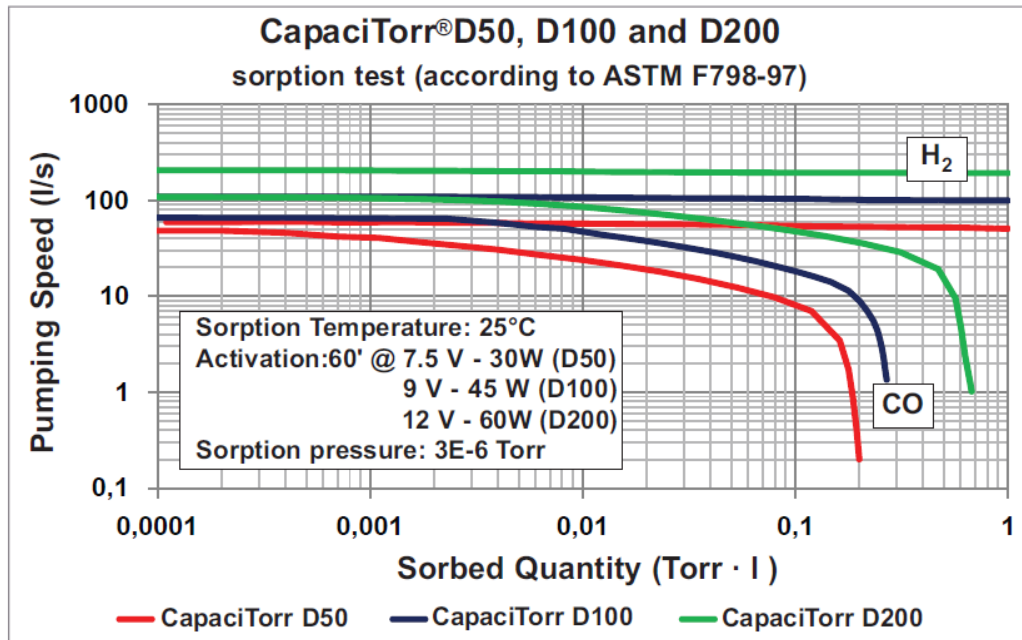


Figure 3.1.5 SAES Capacitorr D200 pumping speed vs sorbed quantity

3.1.3. Total discrete pump speeds

For long tubes molecular flow conductance can be computed by [10]:

$$C_m = 12 * \frac{D^3}{L} \quad (3-1)$$

$$C_{gas} = C_{N_2} * \sqrt{m_{N_2}/m_{gas}} \quad (3-2)$$

Where CN2 is the conductance in liters/second, D is the inner diameter in centimeters, and L is the length in centimeters. The pumps will mount below of a 15.75" long, 2.25" ID tube. Using Equation 3-1 this tube has a nitrogen conductance of 56.0 L/s and then using equation 3-2 the tube has a hydrogen conductance of 209.5 L/s.

The total discrete pump speeds are summed in Table 3.1.1 and then scaled based on the conductance limitations. These pump speeds are applicable for MolFlow+ simulations of 1000 A*hrs beam conditioning or less as the previous calculations expect all pumps to be at full capacity up to that point.

GAS	TITAN 45S-DI PUMP SPEED (L/S)	CAPACITORR D200 PUMP SPEED (L/S)	TOTAL PUMP SPEED (L/S)	CONDUCTANCE REDUCTION (L/S)
H ₂	41.4	200	241.4	112.2
CO	22	100	122	38.4
CO ₂	25.9	100	125.9	33.0
CH ₄	23.3	0	23.3	17.7

Table 3.1.1 Total discrete pump pumping speeds for use in MolFlow+
(@ 1000 A*hrs. or less beam conditioning)

3.2. NEG strips pumping speeds

SAES Getters has provided data for measurements the pumping speed versus sorbed gas quantity for their ST 707/ CTAM/ 30D strip, see Figure 3.2.1. This strip will be employed in the L-bend and straight section chambers of the APS-U MBA storage ring vacuum system. For hydrogen, the pumping speed is near constant at around $900 \text{ cm}^3/\text{s cm}^2$ for all measured quantities. For carbon monoxide, the pumping speed decreases logarithmically with increased sorbed quantity. The x and y axes of the SAES data in Figure 3.2.1 are then converted to more familiar units, L/s/cm^2 and $\text{Torr}^*\text{L/cm}^2$, in Figure 3.2.2.

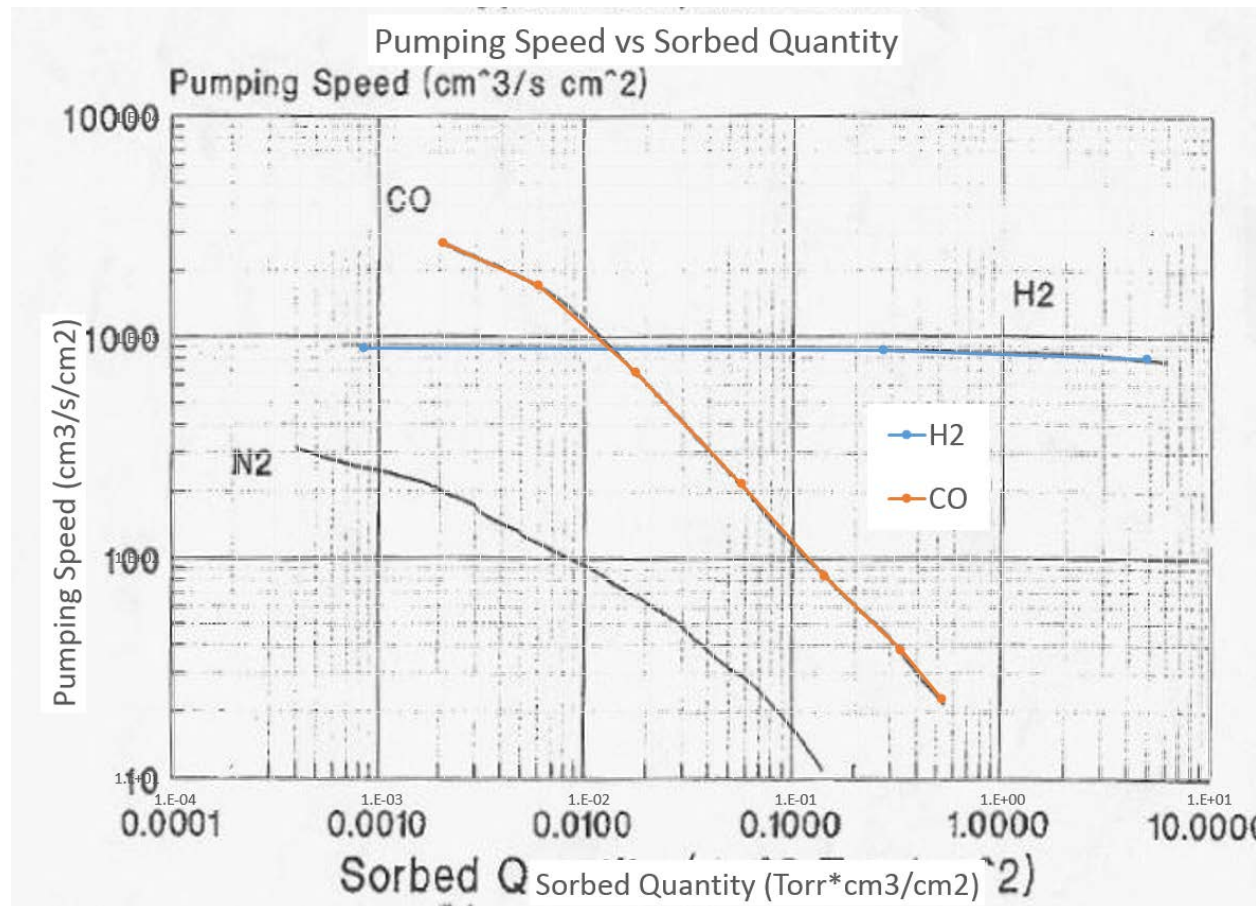


Figure 3.2.1 Pumping speed vs Sorbed Quantity for SAES Getters ST 707/ CTAM/ 30D Strip
(Digitized curves in orange and blue)

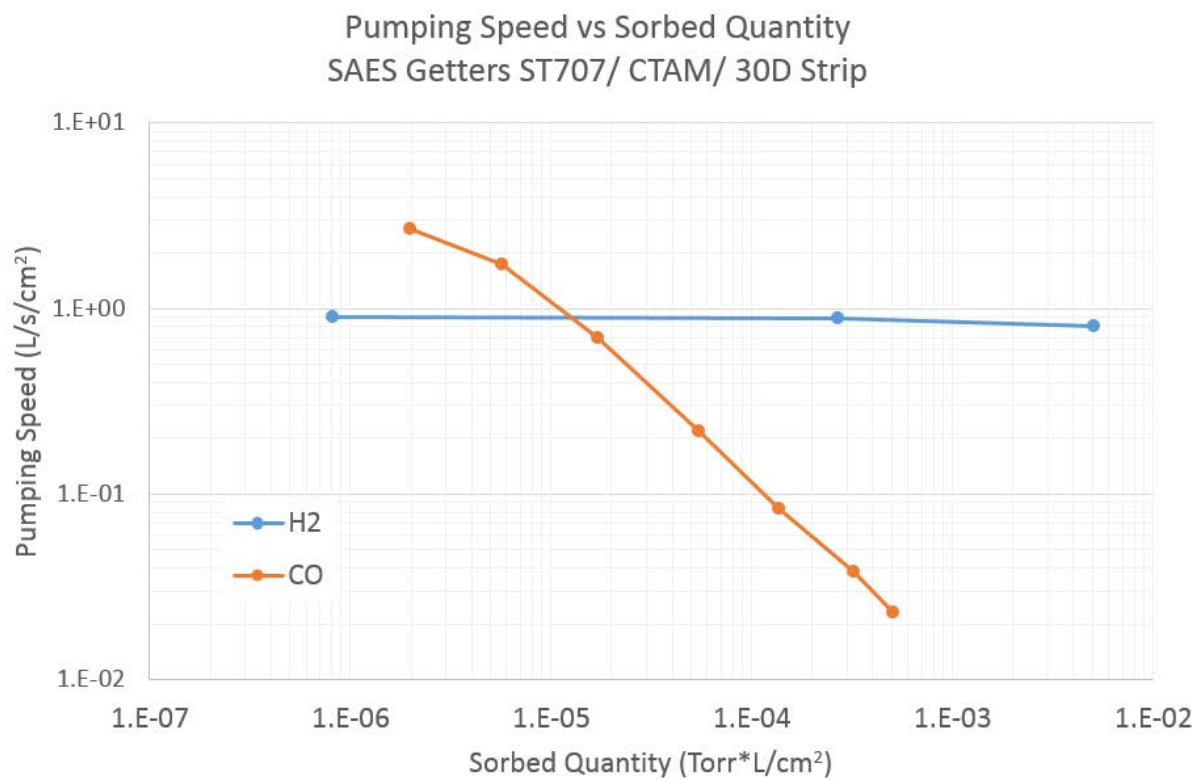


Figure 3.2.2 ST707 Pumping Speed vs Sorbed Quantity

An approximation of the sorbed quantity at the machine operation time of interest must be determined so that an appropriate pumping speed can be applied for vacuum calculations. Hydrogen is typically the dominant gas in quantity in a UHV system with thermal outgassing values for baked metals measured around $1\text{E}-12 \text{ Torr} * \text{L/s/cm}^2$ [11]. For the other significant vacuum gases including carbon monoxide and carbon dioxide the thermal outgassing values for baked metals are around $1\text{E}-13 \text{ Torr} * \text{L/s/cm}^2$ [11].

The surface outgassing rate with beam on is assumed to be an order of magnitude higher than the thermal outgassing rate. This surface outgassing rate is assumed to be near constant for all L-bend surfaces. With this assumption the total gas load can be determined in a typical L-Bend. Then a surface sorption rate can be determined by the two total 2.2m long, 30mm wide NEG strips per L-bend chamber. These calculations are performed in Table 3.2.1 and Table 3.2.2.

	Quantity	Value	Unit	Equation
A	H ₂ 'beam on' outgassing rate	1.00E-11	Torr*L/s/cm ²	approximation
B	L-bend surface area	8.70E+03	cm ²	measured
C	L-bend H ₂ net rate	8.70E-08	Torr*L/s	A*B
D	2x NEG Strip surface area	2.38E+03	cm ²	measured
E	Sorption rate per strip	1.83E-11	Torr*L/s/cm ²	C/D/2

Table 3.2.1 L-Bend chamber NEG strip H₂ sorption rate approximation

	<i>Quantity</i>	<i>Value</i>	<i>Unit</i>	<i>Equation</i>
A	CO ‘beam on’ outgassing rate	1.00E-12	Torr*L/s/cm ²	approximation
B	L-bend surface area	8.70E+03	cm ²	measured
C	L-bend CO net rate	8.70E-09	Torr*L/s	A*B
D	2x NEG strip surface area	2.38E+03	cm ²	measured
E	Sorption rate per strip	1.83E-12	Torr*L/s/cm ²	C/D/2

Table 3.2.2 L-Bend chamber NEG strip CO sorption rate approximation

With a constant sorption rate per strip determined for the L-bend chambers, pumping speeds from the SAES data can be associated with operating times in the system. This is done by dividing the SAES x-axis or the sorbed quantity in units of Torr*L/cm² by the NEG strip sorption rate in units of Torr*L/s/cm² which converts to time units in seconds. The time unit is then converted to operating time units of A*hrs. by multiplying the conversion 1 A*hrs. / 18000 s for a 200 mA operating current. The final conversion of pumping speed versus operating time is shown in Figure 3.2.3.

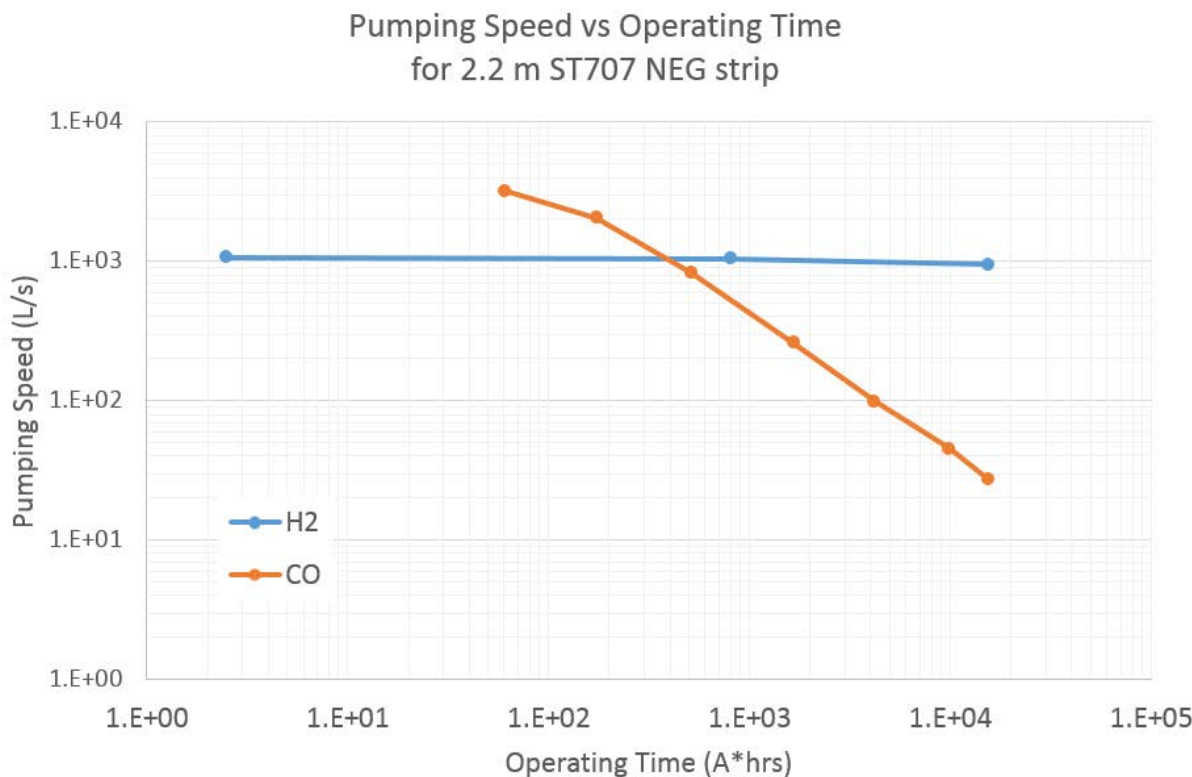


Figure 3.2.3 ST707 Pumping Speed vs APS-U MBA

Pumping speeds for a 2.2m long NEG strip @ 1000 A*hrs. conditioning time are provided in Table 3.2.3 and are based on the above calculations and Figure 3.2.3. From Figure 3.2.3, the H₂ speed is seen to hold near constant at about 1000 L/s per strip. The CO speed reduces with increased sorbed quantity and has a

pumping speed of 400 L/s per strip at 1000 A*hrs. Pumping speed data is not provided for the gases CO₂ and H₂O. The measured curve for CO is assumed to apply for both CO₂ and H₂O and NEG strips are assumed to not pump CH₄. The pumping speeds are applied to the geometry in Figure 3.2.4.

GAS	2.2M NEG STRIP PUMP SPEED @ 1000 A*HRS (L/S)
H ₂	1050
CO	400
CO ₂	400
H ₂ O	400
CH ₄	0

*Table 3.2.3 Pump speeds for MolFlow+ simulation
for a 2.2m long NEG strip @ 1000 A*hrs. operating time*

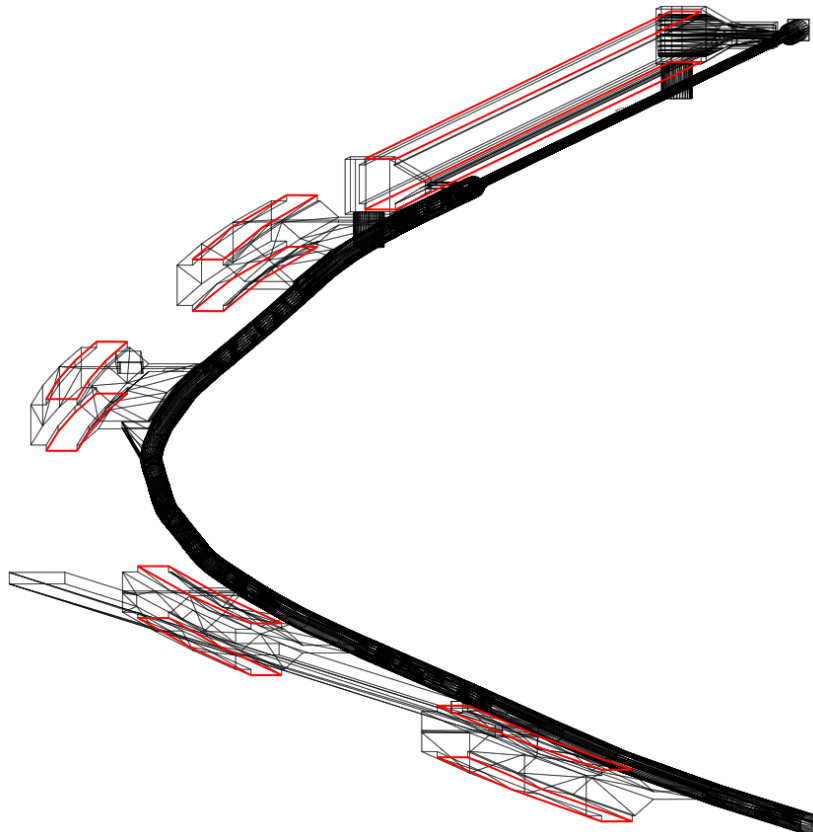


Figure 3.2.4 NEG strip surface area highlighted in red for a MolFlow+ simulation of the APS-U MBA SR vacuum system

3.3. NEG coating pumping speeds

Vacuum properties have been measured for TiZrV non-evaporable getter coatings [11] [12] that are very similar to what are being designed for the APS-U MBA storage ring vacuum system. NEG coating is currently planned to be employed in the FODO section of the storage ring design. A standard coating will be applied to a series of 22 mm ID copper chambers over a span of 4.4 meters. Chiggiato and Costa Pinto [13] showed that sticking factors begin to decrease rapidly after a threshold of about $1\text{E-}5 \text{ Torr}\cdot\text{L}/\text{cm}^2$ CO coverage is met, see Figure 3.3.1. Analysis of the MBA FODO section with MolFlow+ indicated this coverage could be reached at only $10 \text{ A}\cdot\text{hrs}$. This analysis assumes no reactivation of the coating which is contrary to accelerator experience.

In conversations with Roberto Kersevan of CERN [14], he indicated that this early saturation has not been seen in his experiences across multiple facilities. He believes that while the bombardment of photons on NEG coated walls leads to gas release, the same bombardment can reactivate the NEG and release covering molecules. His experience has seen NEG coated chambers last for more than years without seeing significant pumping speed reductions and requiring reactivation.

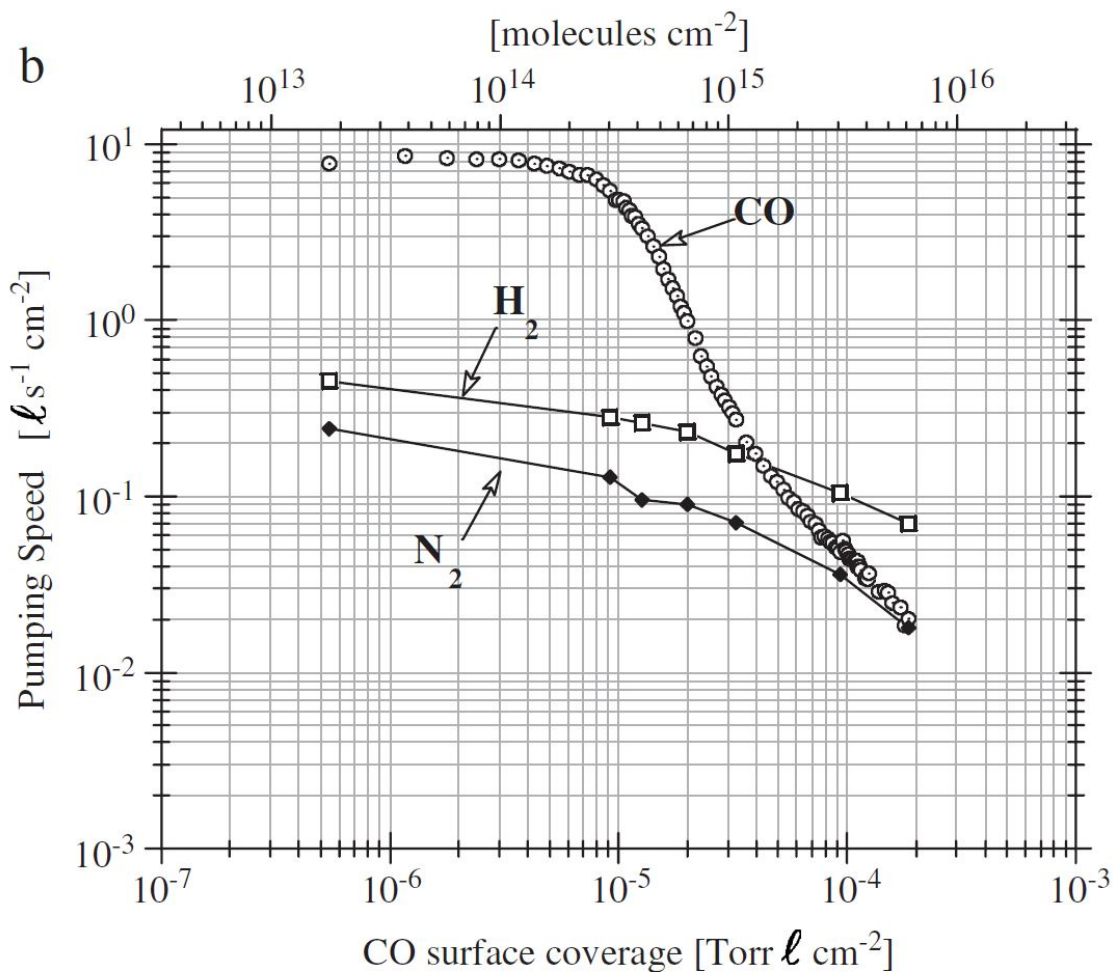


Figure 3.3.1 Ti-Zr-V pumping speed vs CO surface coverage

With this in mind, sticking factors are chosen that are seen prior to saturation in the experiments. Sticking factors, see Table 3.3.1, for H₂ were found to be between 0.006 and 0.05. The lowest value will be taken to be conservative. For CO, sticking factors were found to be high in the first order of magnitude. To be conservative, 0.1 will be taken and is assumed to apply for CO₂ and H₂O as well. NEG coating is assumed to not pump CH₄. The sticking factor is applied to the geometry in Figure 3.3.2.

VACUUM GAS	NEG COATING STICKING FACTOR	FODO SECTION NEG COATING TOTAL PUMPING SPEED (L/S)
H ₂	0.006	800
H ₂ O	0.1	4460
CO ₂	0.1	2850
CO	0.1	3580
CH ₄	0	0

Table 3.3.1 NEG Coating sticking factors for MolFlow+ simulations

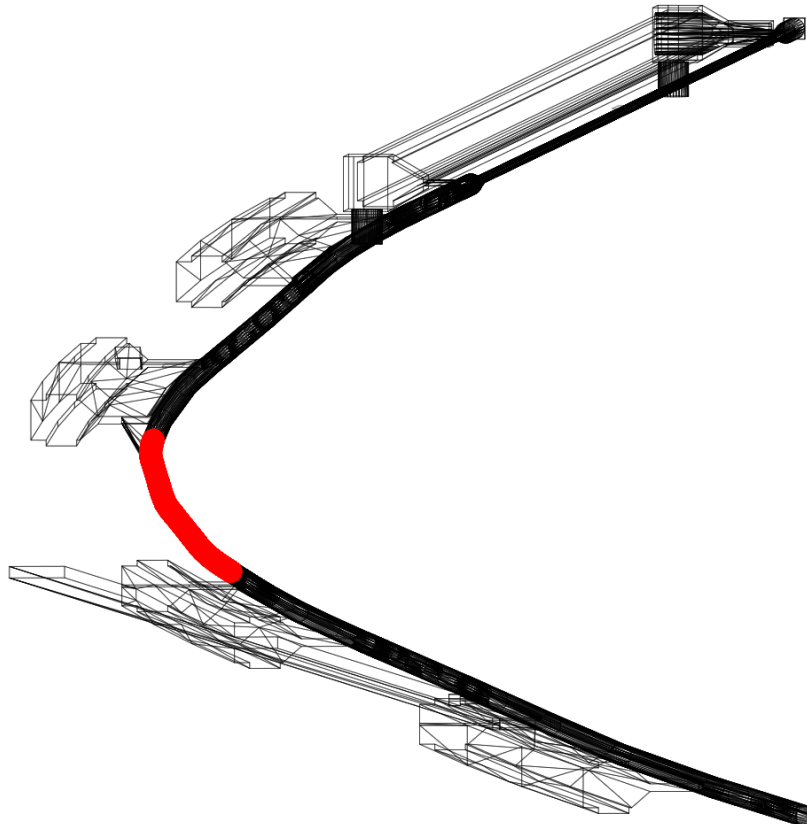


Figure 3.3.2 NEG coated surface area highlighted in red for a MolFlow+ simulation of the APS-U MBA SR vacuum system, ~2940 cm² approximate surface area of chambers

4. Photon stimulated desorption in MolFlow+

Photon stimulated desorption (PSD) is assumed to be the dominant outgassing load when the beam is on in the MBA storage ring vacuum system. PSD can be estimated in the SynRad/MolFlow+ programs through a process that computes SynRad generated photon fluxes on surfaces and converts them to PSD outgassing. The conversion is determined per material and is based on experimental data. The sections below provide details about the experiments and how their data is converted for us in MolFlow+ simulations.

4.1. Notes about PSD yield experiments

Foerster [15] has collected data from PSD yield experiments for common vacuum materials including aluminum, copper, and copper plated stainless steel. These experiments were all performed using nearly identical experimental setups at either the U10B or X28A beamline at NSLS. A schematic of the two beamlines and their respective experimental setups are shown in Figure 4.1.1 and Figure 4.1.2. Chiggiato and Kersevan [16] collected the same data for a NEG coated chamber using a similar experimental setup at the D31 beamline at ESRF, see Figure 4.1.3 for beamline schematics.

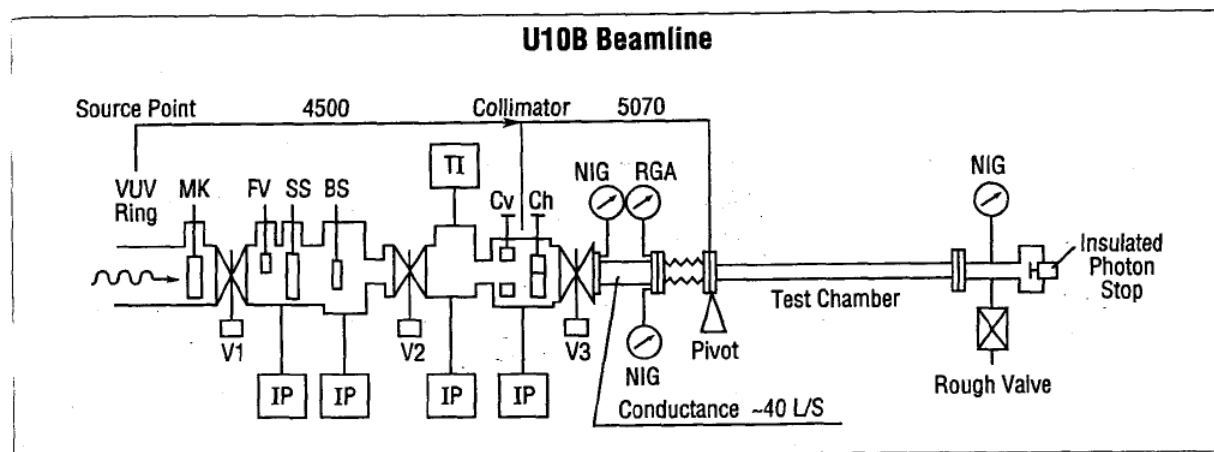


Figure 1. Schematic diagram of NSLS Beamline U10B and the test chamber setup: MK - Mask; FV - Fast Valve; SS - Safety Shutter; BS - Beam Stop; Cv + Ch - Vertical and Horizontal Collimator; T1 - Titanium Sublimation Pump; NIG - Nude Ion Gauge; IP - Ion Pump; RGA - Residual Gas Analyzer; and V1, V2, V3 - All Metal Valves. Distances from the source point are in mm.

Figure 4.1.1 PSD yield experimental setup at the U10B beamline at NSLS

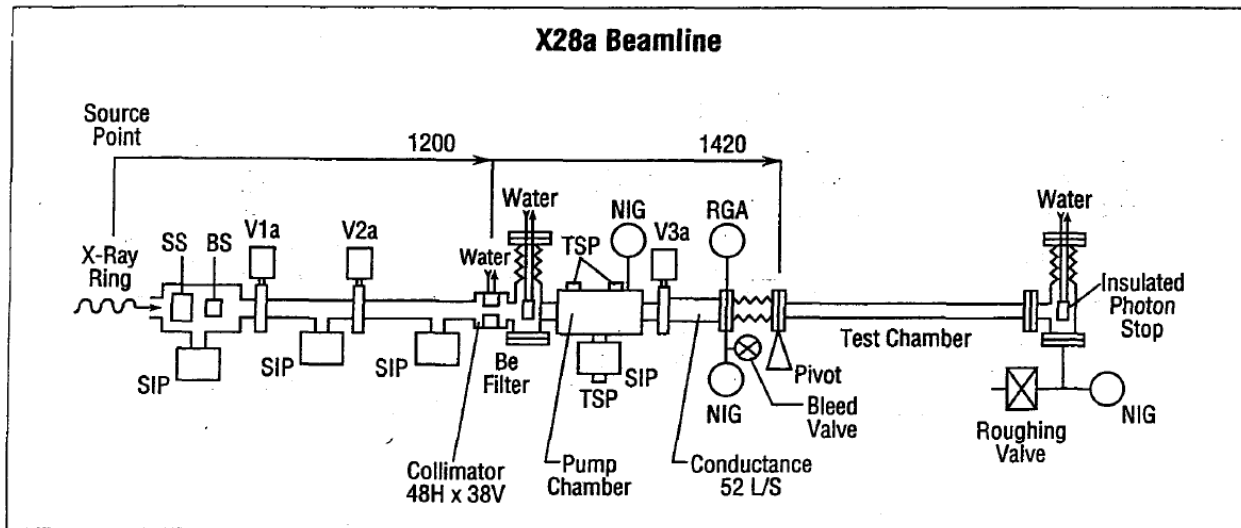


Figure 2. Schematic diagram of NSLS beamline X28A and test chamber set up: SS - Safety Shutter; BS - Beam Stop; SIP - Sputter Ion Pump; TSP - Titanium Sublimation Pump; NIG - Nude Ion Gauge; RGA - Residual Gas Analyzer; V1a, V2a, V3a - All Metal Gate Valves. Distances from the source point are in cm.

Figure 4.1.2 PSD yield experimental setup at the X28A beamline at NSLS

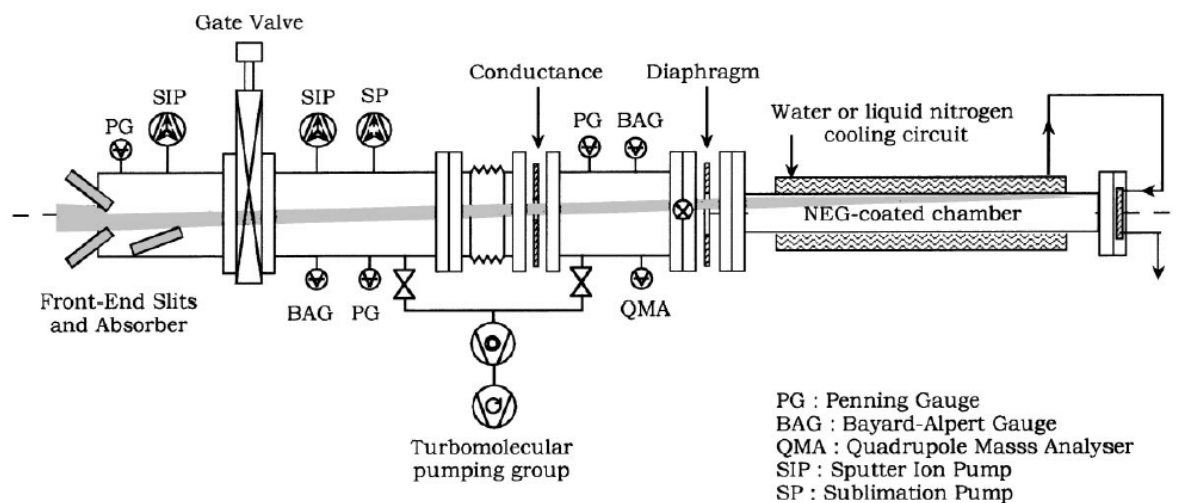


Fig. 1. Schematic view of the D31 beamline vacuum system.

Figure 4.1.3 PSD yield experimental setup at the D31 beamline at ESRF

The experiments expose a chamber to a known, collimated photon source and record the change in pressure as the photon accumulation increases. The change in pressure is converted to change in outgassing and the ensuing data generally forms a curve with two behaviors. The first behavior is a near constant yield rate at lower flux accumulations until a ‘low flux cutoff’ is reached. This low flux cut off has generally been seen at accumulation values of around 1E20 photons/meter. After this a surface clean up begins that which follows a power law. The data from these experiments will be digitized for each material relevant to the

MBA storage ring vacuum system and a two part curve will be approximated which includes the constant yield and power law behaviors.

While many papers exist for a variety of popular UHV materials with a variety of surface preparations, there have not yet been enough experiments performed to develop any standard. A close fit of the power law is still be valuable and can provide predictions of the dynamic outgassing load within the complex system.

4.2. Importing PSD outgassing into MolFlow+

The goal of coupled SynRad/MolFlow+ simulations is to predict the dynamic photon stimulated desorption outgassing and thus predict dynamic pressures within an accelerator vacuum system. An accurate prediction of the outgassing requires two steps: first an accurate SynRad simulation of the photon flux distribution such as in Figure 4.2.1 which will be discussed in Section 5, and second, and equally as important, a means to map the SynRad flux distributions onto a MolFlow+ model as dynamic PSD outgassing.

MolFlow+ provides a tool for importing SynRad flux textures into an equivalent geometry model and mapping them as PSD outgassing as shown in Figure 4.2.2. The tool requires two pieces of information: a time in seconds which represents an equivalent time for the machine at full max current to reach a desired conditioning point in Amp*hours, and a map file for converting the photon flux densities computed at each mesh point in SynRad to an outgassing value.

The map file is a calibrated function which should compute outgassing values similar to the original PSD measurement. Creating the file requires two steps: first recreating the experiment in SynRad, and second iterating a function that reproduces gas loads similar to the original experimental data. The ray trace from a typical PSD measurement is shown in Figure 4.2.4 and highlights the purpose of irradiating a chamber with a controlled photon load over a fixed length of the chamber. Figure 4.2.4 and Figure 4.2.5 show how the photon ray trace can be recreating within a similar SynRad model and then flux densities can be computed with the added calculation of secondary photon scattering to include the outgassing contribution of all chamber surfaces. Lastly, Figure 4.2.6 diagrams the calibration of the final function. The calibration starts with an initial guess, usually the original data with an x-axis of ‘photons/meter’. The calibration is complete when a new function is determined that maps spatial photon densities (with units of photons/cm²) to outgassing loads near equivalent to the original experiment.

The following subsections detail the recreation of each experiment corresponding to the variety of materials incorporated in the vacuum system design.



Figure 4.2.1 Example log scale flux density rate (photons/second/cm²) map computed for a SynRad simulation with photon scattering

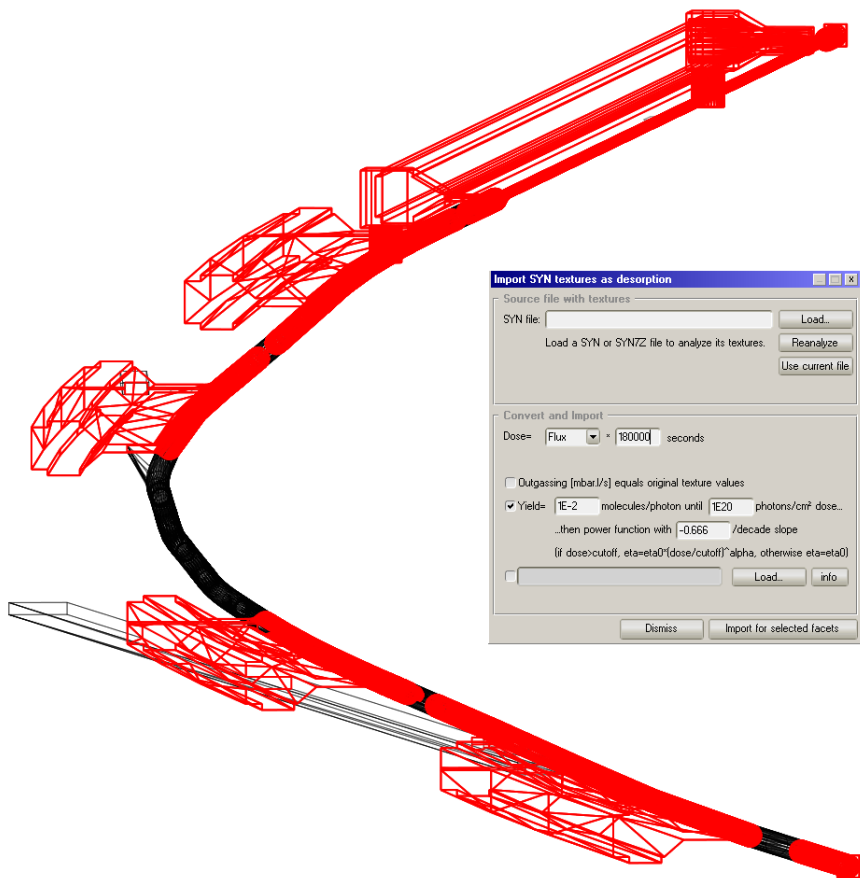


Figure 4.2.2 MolFlow+ (v 2.5.6) menu for translating a SynRad flux map into PSD outgassing

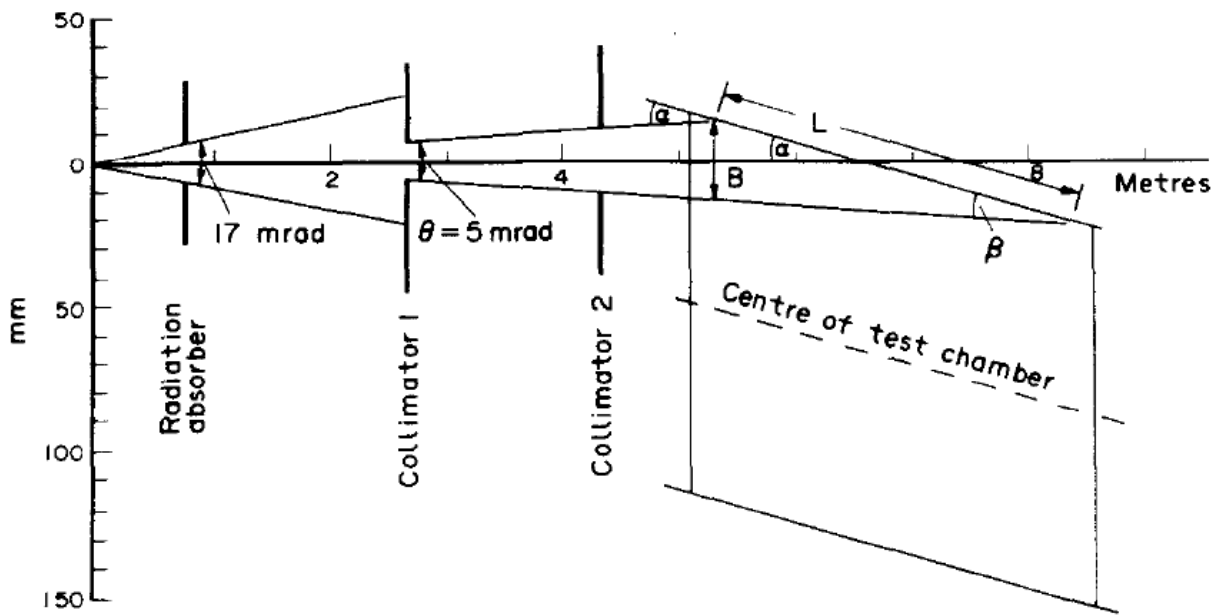


Figure 4.2.3 Typical ray trace for design of a laboratory PSD measurement

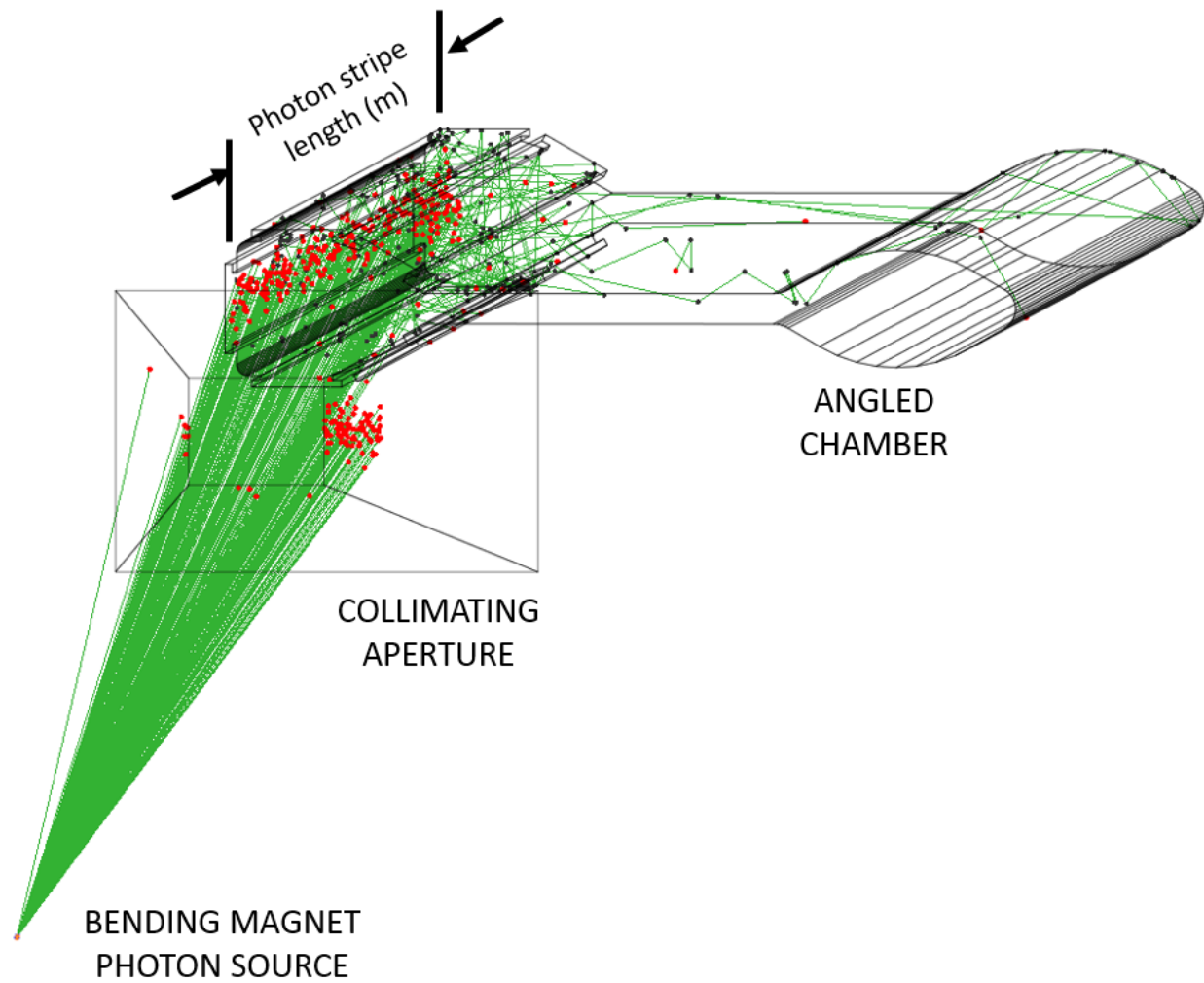


Figure 4.2.4 Ray trace from a PSD measurement recreated in SynRad with photon scattering

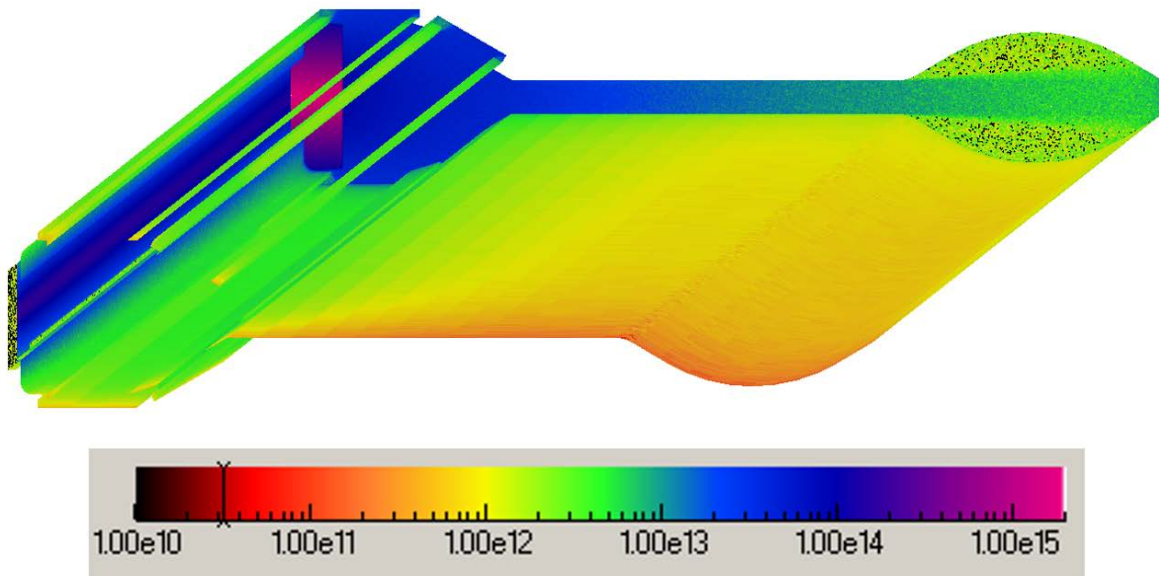


Figure 4.2.5 SynRad photon flux densities computed for the recreation of a typical PSD measurement

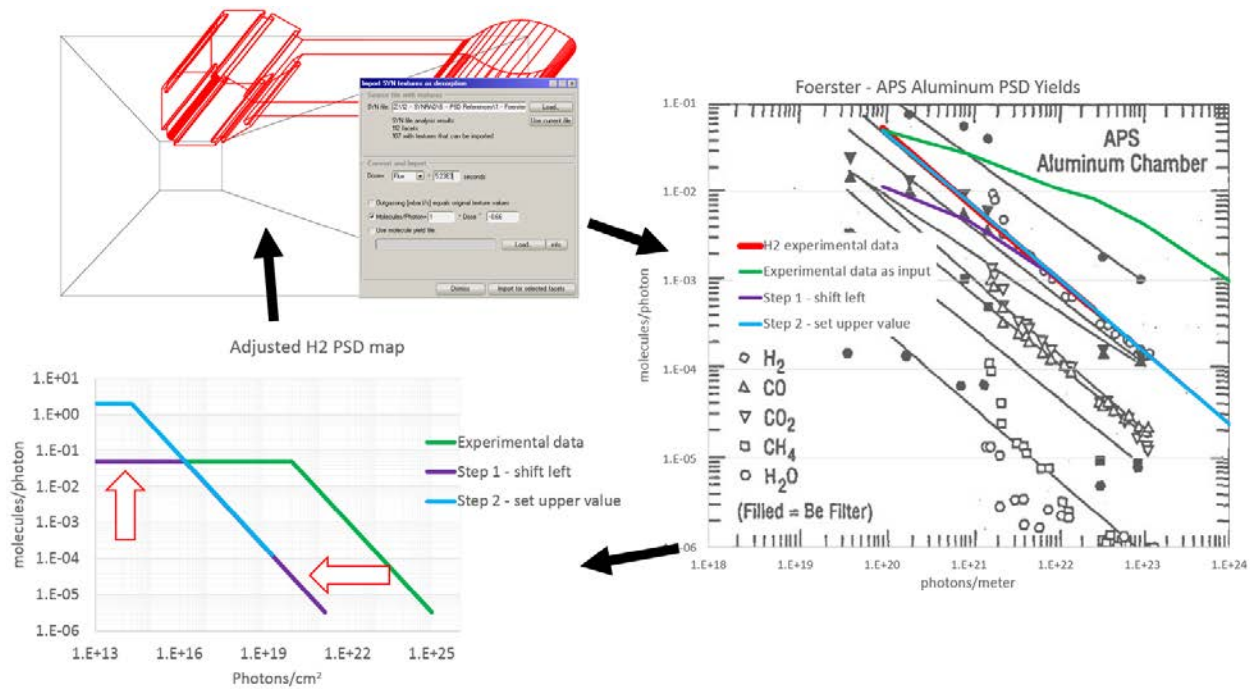


Figure 4.2.6 Diagram of iterative process for calibrating PSD yields for use in MolFlow+ where the approximated PSD functions are used to map the fluxes from Figure 4.2.18 to outgassing in MolFlow+. The functions are adjusted until the predicted outgassing matches the original data

4.2.1. Aluminum outgassing map

Aluminum surfaces represent over 90% of the surface area in the APS-U storage ring vacuum system design so a study will be performed comparing the use of four separate published PSD measurements [15] [16] [17] [18]. The PSD measurements were taken by separate groups on chambers with a variety of cross sections. Three of these cross sections are highlighted in Figure 4.2.7. The results from the four measurements are shown in Figure 4.2.8, Figure 4.2.9, Figure 4.2.10, and Figure 4.2.11. Figure 4.2.12 shows a comparison of the variety of chamber geometries recreated in CAD. Three of the chambers feature antechambers and two feature pumping slots between the antechamber and beam aperture. Figure 4.2.13 shows the ray traces for the four separate experiments recreated in SynRad with photon scattering.

Figure 4.2.14 shows a comparison of the H₂ portion of the four measurements. Here it can be seen that the range of data varies between the four measurements and that the chambers seem to have similar clean up slopes but slightly different magnitudes of yield. The largest variation between the four experiments appears to be the size and complexity of the four geometries measured and may be the key cause for the variety of results. The bake-out conditions for the four experiments were generally similar although not identical. The four chambers were likely made from extruded aluminum but the complete manufacturing details of the chambers are not yet known.

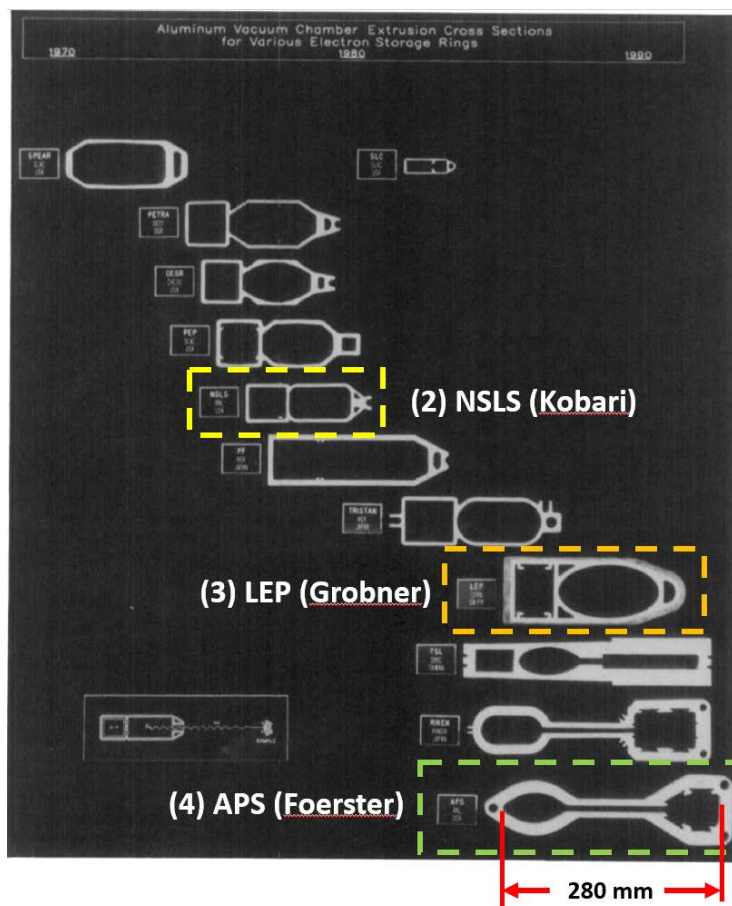


Figure 4.2.7 Comparison of three of the four aluminum chamber cross sections with published PSD measurements

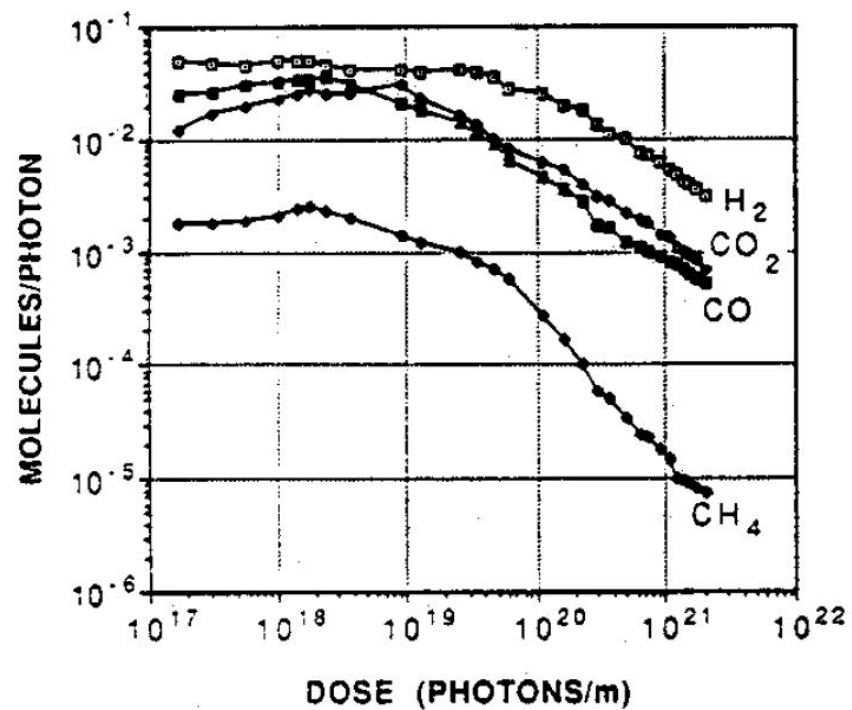


Figure 4.2.8 Mathewson PSD measurement from an elliptical aluminum chamber

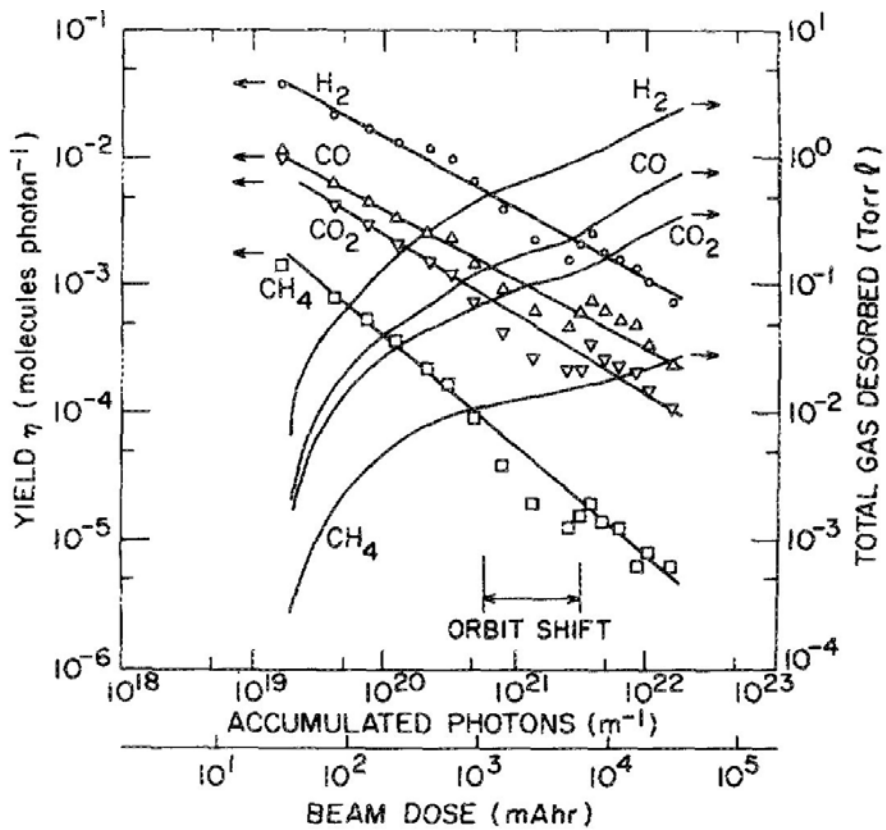


Figure 4.2.9 Kobari PSD measurement from an aluminum NSLS extrusion

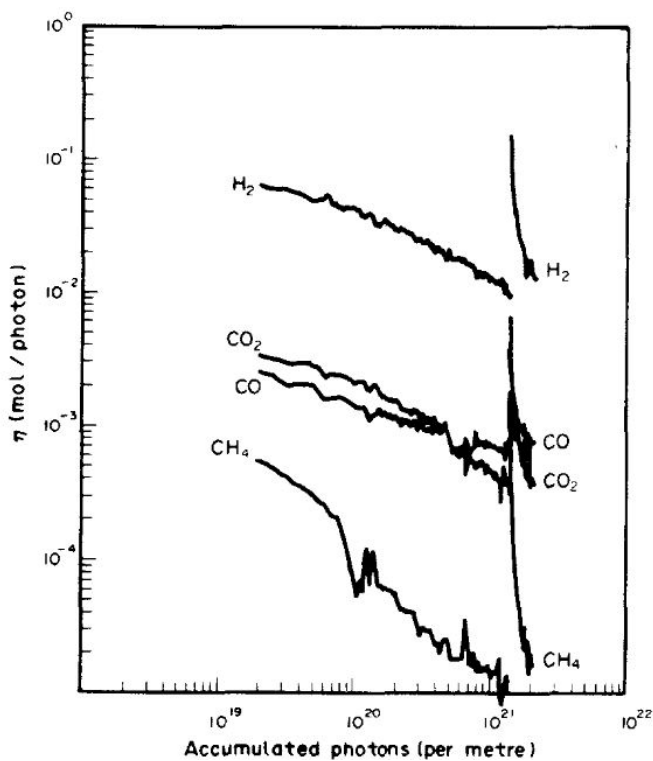


Figure 4.2.10 Grobner PSD measurement from an aluminum LEP extrusion

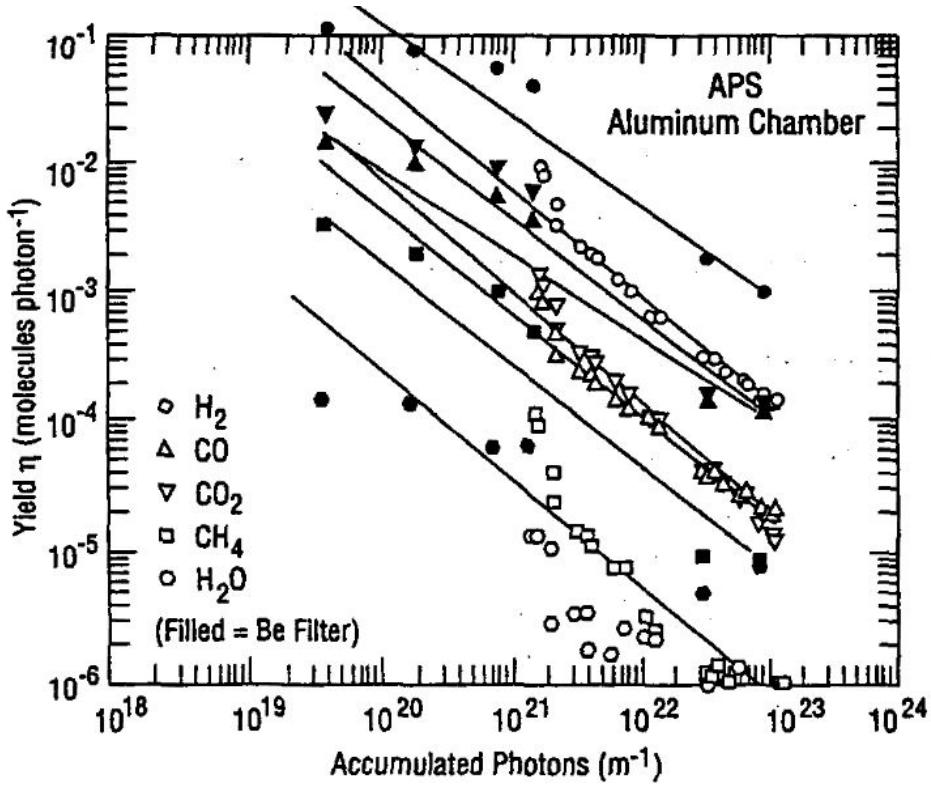


Figure 4.2.11 Foerster PSD measurement from an aluminum APS extrusion

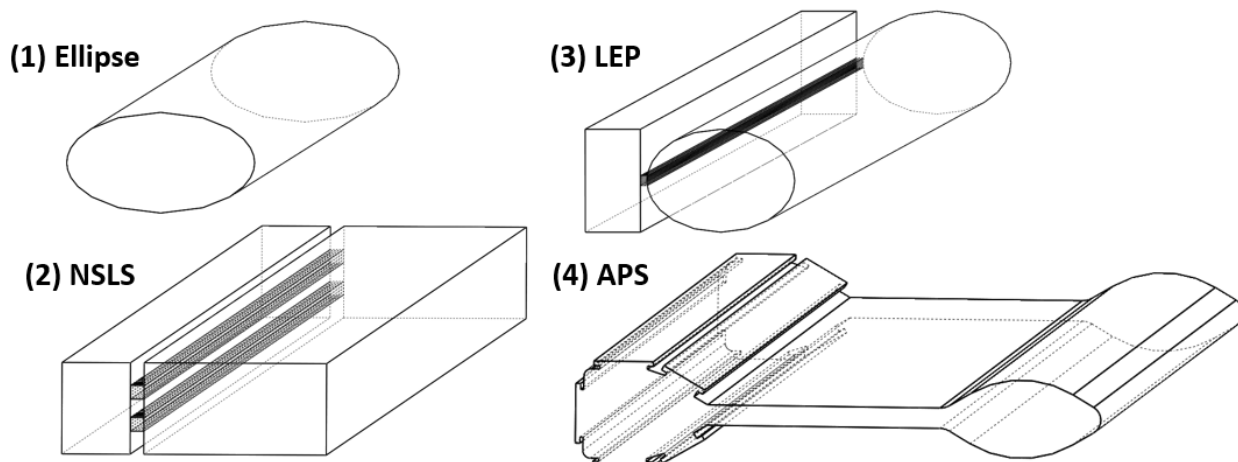


Figure 4.2.12 CAD models of the four chamber geometries for use in MolFlow+

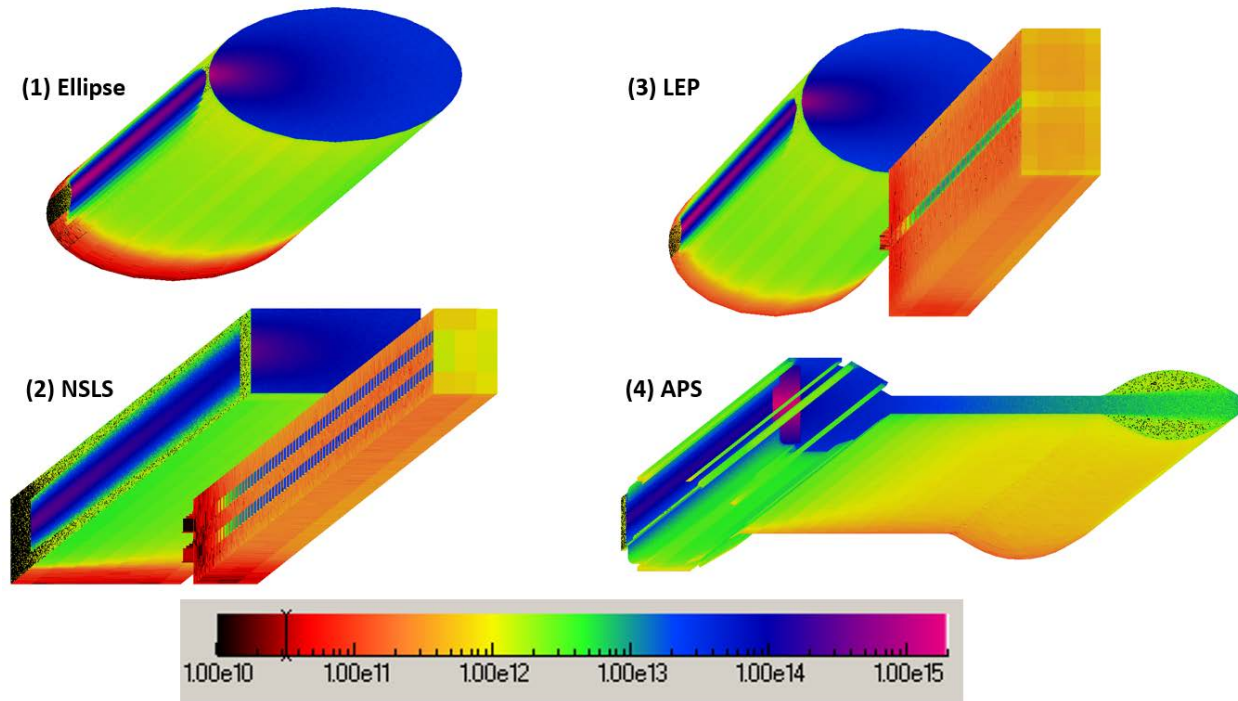


Figure 4.2.13 Four aluminum PSD measurements recreated in SynRad with photon flux densities (photons/cm²/s) in log scale

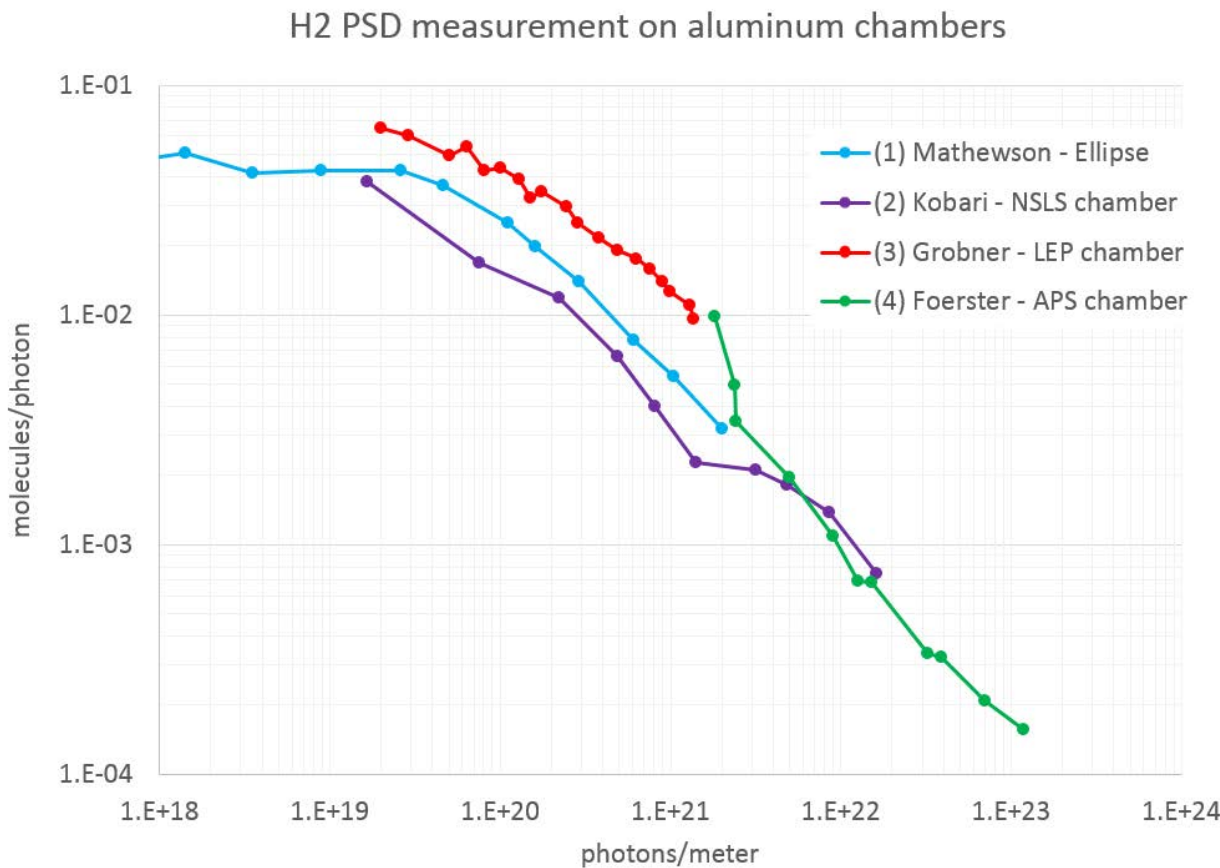


Figure 4.2.14 Comparison of four published H₂ PSD yields measured on various aluminum chambers

4.2.2. OFHC copper outgassing map

The PSD yield measurement experiment for an OFHC copper chamber [19] was recreated in SynRad, see Figure 4.2.15. The experiment was performed at the X28A beamline at NSLS. The chamber tested was a 3 meter long C10100 extruded copper and was fabricated to the B-factory cross section design. The chamber was exposed to a dose greater than 10^{23} photons/meter at a 25 degree angle and 14.2 meter distance by white light with a critical energy of 5 keV from the 2.5 GeV, 500 mA storage ring. The results from the PSD measurements are shown in Figure 4.2.16.

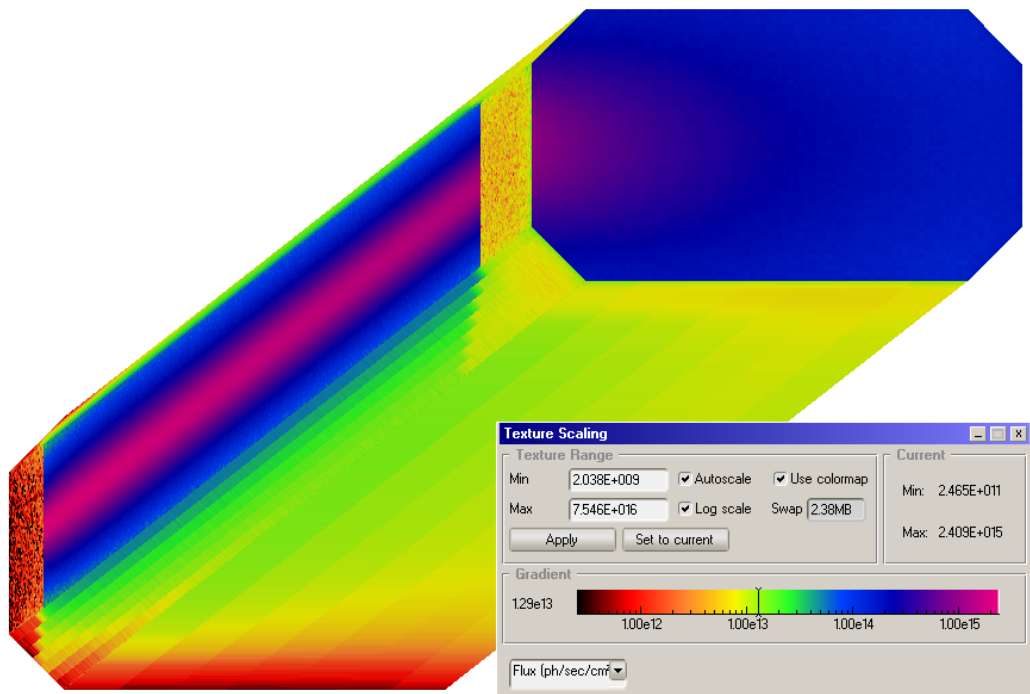


Figure 4.2.15 Copper chamber PSD measurement experiment recreated in SynRad

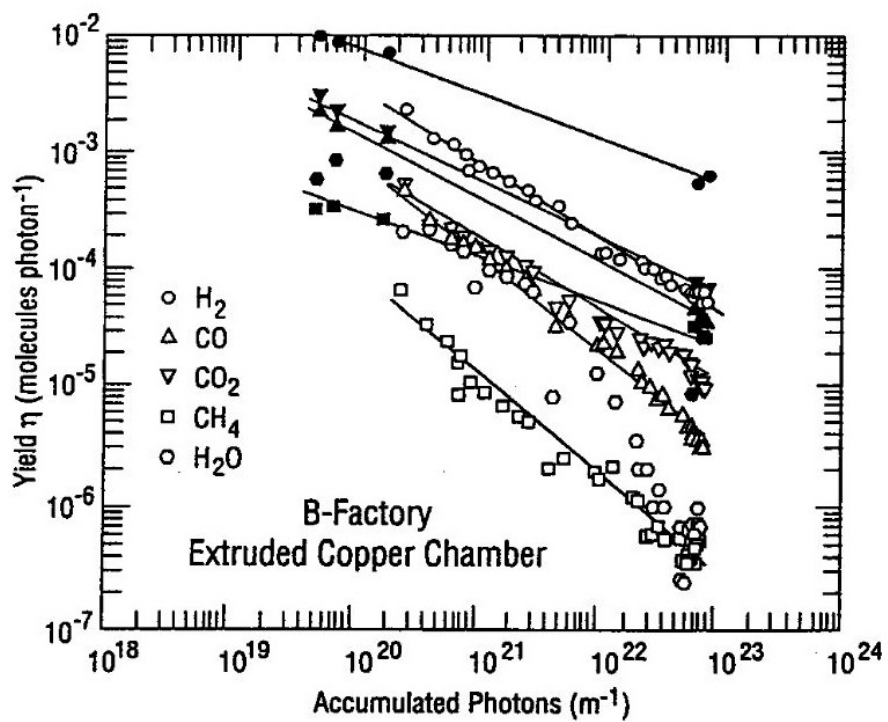


Figure 4.2.16 PSD measurement from an OFHC copper PEP-II style vacuum chamber

4.2.3. Cu-plated stainless steel outgassing map

The PSD yield measurement experiment for a Cu-plated stainless steel chamber [20] was recreated in SynRad, see Figure 4.2.17. The experiment was performed at the U10B beamline at NSLS. The chamber tested was a 3 meter long, 30.4 mm ID, Cu-plated stainless steel tube. The chamber was exposed to a dose greater than 10^{22} photons/meter at a 10 degree angle and 5.07 m distance from a white light source with a critical energy of 0.5 keV from the 0.75 GeV, 1000 mA storage ring. The results from the PSD measurements are shown in Figure 4.2.18.

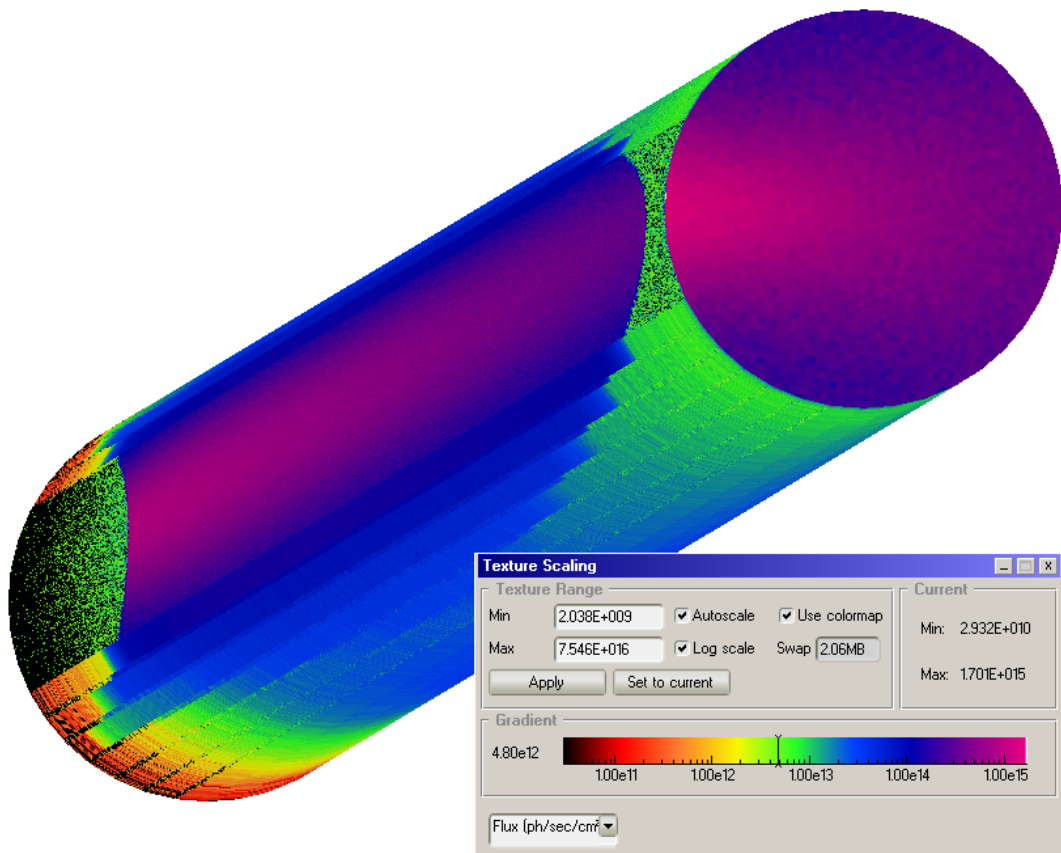


Figure 4.2.17 Cu-plated stainless steel PSD measurement experiment recreated in SynRad without photon scattering

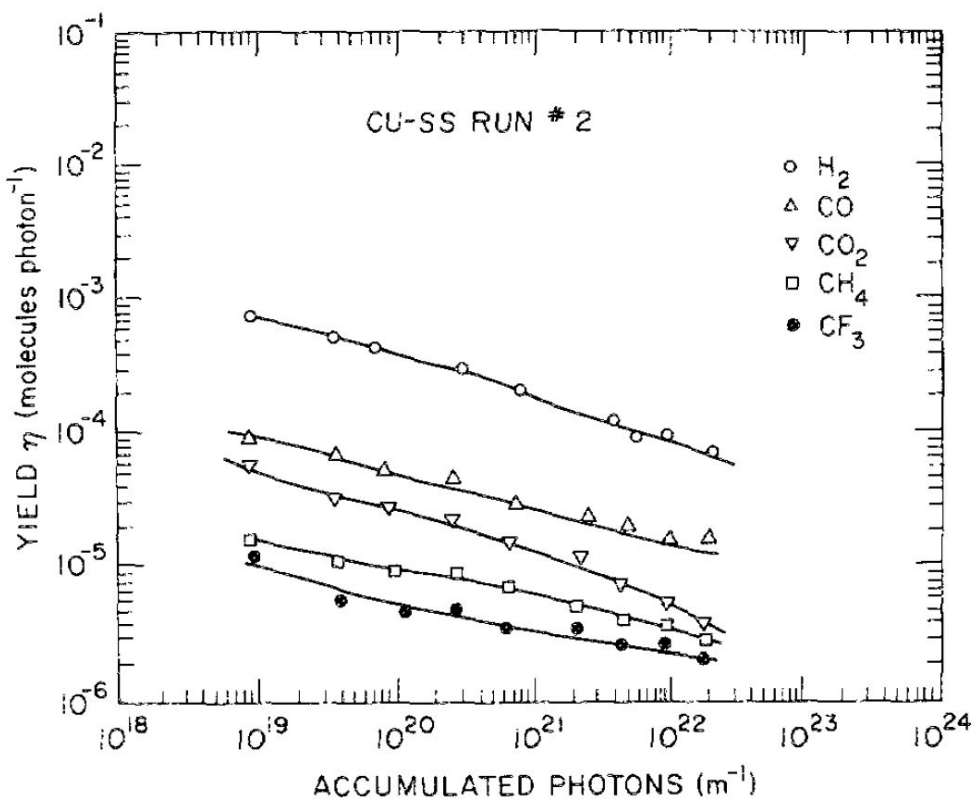


FIG. 7. Molecular desorption yields for *in situ* baked copper-plated stainless steel.

Figure 4.2.18 PSD yield vs accumulated photons for a copper plated stainless steel vacuum chamber

4.2.4. NEG coated stainless steel outgassing map

The PSD yield measurement experiment for a NEG coated stainless steel chamber [14] was recreated in SynRad, see Figure 4.2.19. The PSD measurements from the paper were digitized and plotted over the original data in Figure 4.2.20. The exact gas composition of the total yield measurement was not reported so the APS storage ring composition was assumed. The experiment was performed at the D31 beamline at ESRF. The chamber tested was a 2 meter long, 60 mm ID, NEG coated 316LN stainless steel tube. The chamber was exposed to a dose greater than 10^{23} photons/meter at a 25 degree angle and 8.27 m distance from a white light source with a critical energy of 20.5 keV from the 6 GeV, 185 mA storage ring.

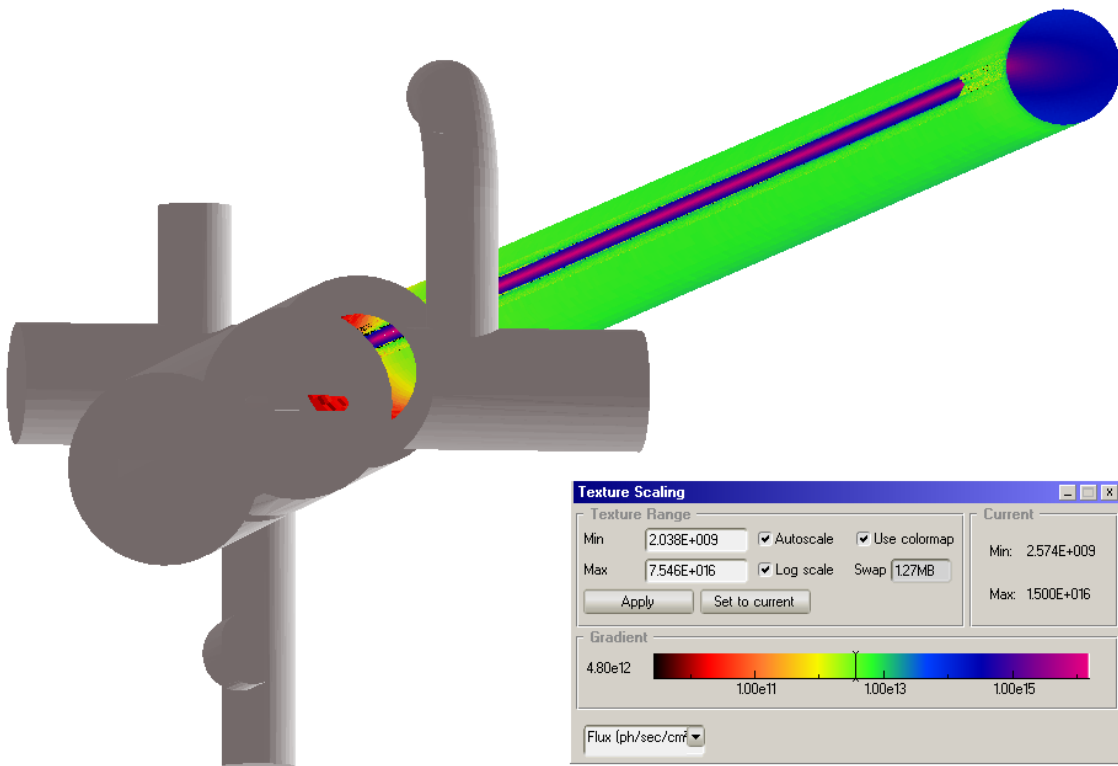
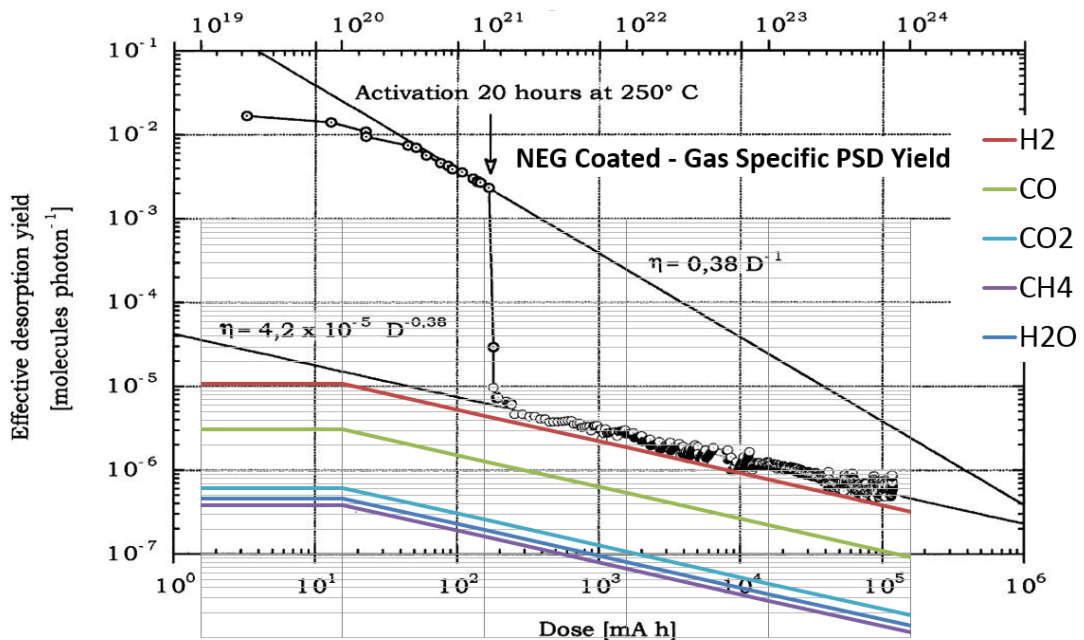


Figure 4.2.19 NEG coated stainless steel PSD measurement experiment recreated in SynRad without photon scattering



molecular desorption yield η (N_2 equivalent) of the Ti-Zr-V coated stainless-steel chamber as a function before and after activation.

Figure 4.2.20 PSD yield vs accumulated photons for a NEG coated stainless steel vacuum chamber

5. SynRad simulation and results

A SynRad simulation generates a steady state flux density rate map on the metallic vacuum interior surfaces. Photon scattering is included in the simulation and is defined at each surface by definitions of both material and surface roughness and by incident angle of the contacting photon. The computed flux density map is then mapped into a MolFlow+ model as a dynamic PSD outgassing load.

5.1. SynRad model assumptions

Material reflection tables are provided in SynRad for the materials aluminum and copper and are generated with data from the Berkeley Center for X-Ray Optics [21]. Surfaces that represent OFHC, copper-plated stainless steel, and NEG coated materials are assigned with copper reflectivity. The rest of the surfaces are assumed to be aluminum and are assigned with aluminum reflectivity.

A single global surface roughness ratio is applied for all of the metallic vacuum surfaces. The roughness ratio is defined as the RMS roughness divided by the correlation length. A ratio of 0.308 is applied uniformly to all surfaces and was determined from measurements on unpolished APS Aluminum extrusions [22].

Bending magnet source definitions are defined with data from lattice file: ‘H7BA-TwoSector-nux95-nuy36-3PW-Version6’. The bending magnet definitions represent the 7 bending magnets in each MBA sector: M1, M2, M3, and M4 and then in reverse M3, M2, and M1 again. The input parameters for each magnetic source include:

- Geometry and orientation: start position and direction, magnet length
- Particle settings: electron, particle mass
- Beam parameters: storage ring energy, beam current, emittance, coupling, BetaX, BetaY, Eta, Eta prime, and Energy spread
- Photon information: Minimum and maximum photon energy range
- Magnetic field value

The physical values from the lattice file that define each individual bending magnet regions are used as direct inputs into SynRad.

5.1.1. Photon reflectivity in SynRad

SynRad version 1.3.3 was used for photon generation and scattering predictions. For models with photon scattering, SynRad requires a material reflectivity definitions for each surface of the model. SynRad provides options for the vacuum materials aluminum and copper which then references reflectivity tables from data measured at the Berkeley Center for X-Ray Optics. More details about the data and algorithms employed to reflect photons are provided at the SynRad/MolFlow website [1]. For the APS-U model, all surfaces are assumed to have the reflectivity of aluminum or copper. NEG coated surfaces are assumed to reflect photons like copper. Figure 5.1.1 and Figure 5.1.2 plot the reflectivity table data that is employed in SynRad for aluminum and copper surfaces.

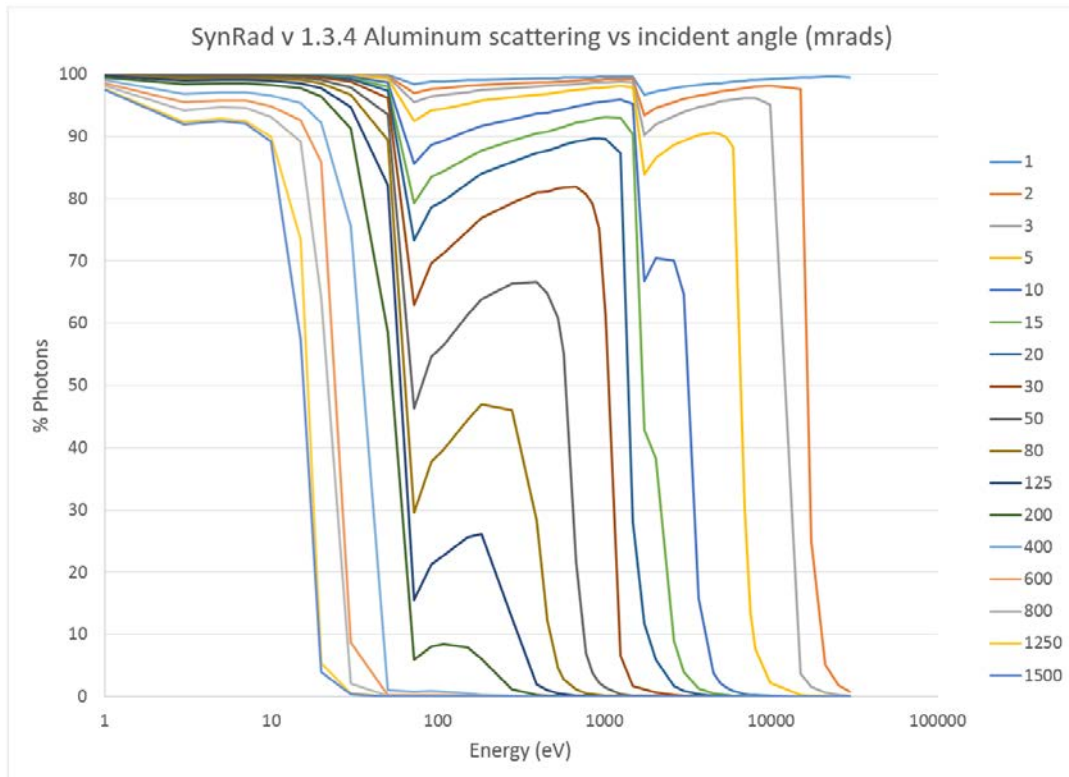


Figure 5.1.1 Aluminum surface reflectivity in SynRad

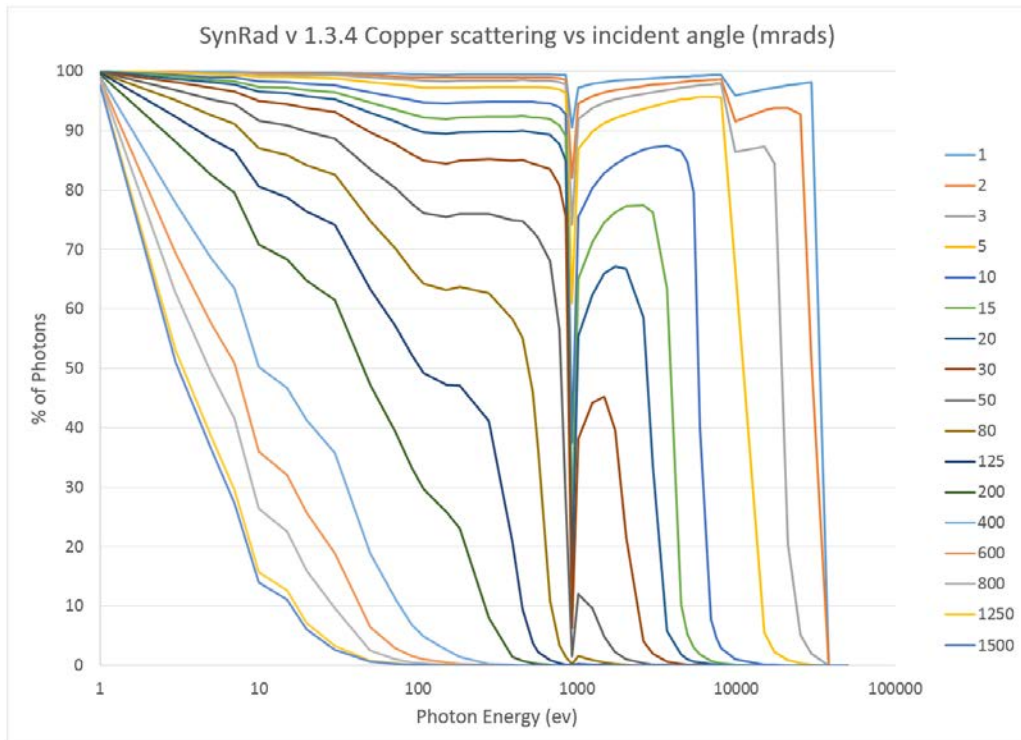


Figure 5.1.2 Copper surface reflectivity in SynRad

5.2. SynRad Results

Figure 5.2.1 shows a view of the steady state photon flux density rate map computed on the interior surfaces of a model of the MBA storage ring vacuum system. A hybrid mesh is employed to capture the varying flux gradients while minimizing computer resources. Fine mesh densities with ~0.1 mm square length are used at locations of primary beam incidence to capture the high gradient of the fine beam profile. Coarser mesh densities of about 10mm square length are used in the majority of the geometry to capture the much lower gradients of secondary flux.

The total flux generated by the 41pm V1.5 lattice magnetic regions is 2.66E19 photons/sec. The total power generated by the V6 magnetic regions is 13.7.



*Figure 5.2.1 SynRad steady state flux density rate distribution in photons/s/cm²
(log scale over 8 orders of magnitude)*

5.3. Comments on results

The shielding in the MBA storage ring vacuum system is designed so that the beam is only intercepted at compact absorbers therefore avoiding long ‘stripes’ of beam on bare metal chamber walls, see Figure 5.2.1. The purpose of this is to avoid the consequences of high bare metal PSD outgassing distributed over long lengths. This current shielding arrangement cannot completely shield all bare walled chambers and this problem is most pronounced in chambers without distributed pumping such as in the multiplets. The compact beam absorbers are located as close to pumps as possible in order to keep ensuing pressures as low as possible. The exceptions for this are the NEG coated FODO section chambers where the low PSD desorption property of NEG coating allows for the chamber walls to collect beam as a distributed absorber without the consequence of high outgassing, see Figure 5.2.2.

Figure 5.2.1 and Figure 5.2.2 both show a ‘top cut off’ view that reveal the interior vacuum surfaces. The plots are in log scale and have a range of about 10 orders of magnitude, from 10^9 to 10^{19} photons/sec/cm 2 . The high end of the scale represents primary beam incidence on chamber and absorber walls and the low end of the scale represents regions that receive very little photon flux after beam scattering. Primary beam incidence can be seen at absorber regions or the FODO section chamber walls in the blue to pink color range of the gradient.

High secondary flux concentrations that scatter from absorbers can be seen in the yellow to green color range. Some fluxes in the green range are seen along the top and bottom walls of the straight-section pumping aperture. This is due to some small but perhaps not insignificant beam scraping of the ‘tails’ of the vertical beam profile which is more pronounced near the end of the long 5.8m chamber length where the source has been allowed to spread the most. Future designs will address this by either changing the aperture gap or providing upstream vertical shielding closer to the source.

Much lower flux concentrations are seen in well shielded or far from absorber regions in the black to orange color range. The low flux concentrations are important to compute because their translated PSD outgassing has been seen to be higher than the $\sim 1E-12$ mbar*L/s/cm 2 rate that would be assumed for thermal outgassing.

The maps from the two figures are then mapped into a MolFlow+ model as a dynamic PSD surface outgassing.

6. MolFlow+ simulation and results

A MolFlow+ model is created by adding pumping elements to the same interior surface geometry from the SynRad model. The SynRad computed steady state flux density rates are then mapped onto the MolFlow+ surfaces as a dynamic PSD outgassing load at a given beam conditioning time. Finally, gas specific pressure profiles are computed along the center of the beam path. Section 3 lists the pumping speeds and pumping element locations for the MolFlow+ model. Section 4 covers the details of photon stimulated desorption calculations.

6.1. PSD outgassing import

Figure 6.1.1, Figure 6.1.2, and Figure 6.1.3, shows where various vacuum materials are found for the PSD import process. Table 6.1.1 compares outgassing @ 1000 A*hrs computed using the four separate aluminum PSD measurements.

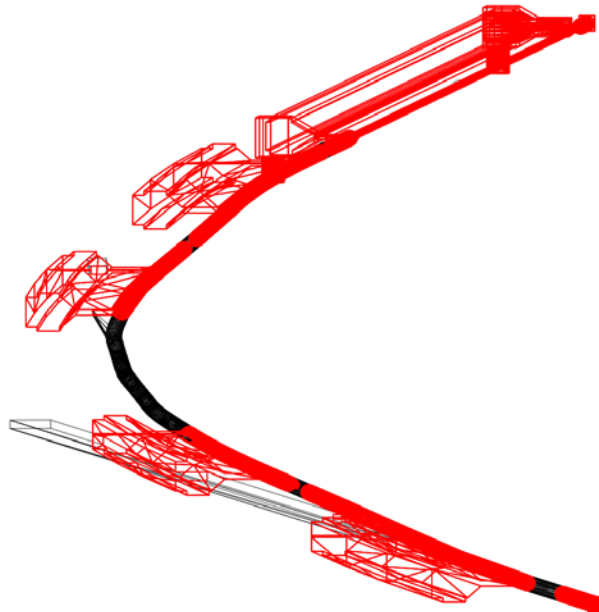


Figure 6.1.1: Aluminum surfaces for PSD import

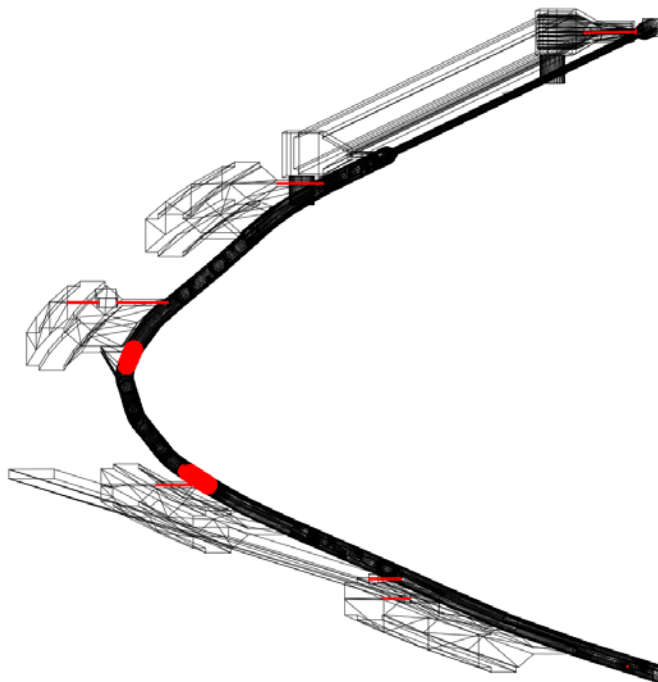


Figure 6.1.2 Oxygen free copper (OFHC) surfaces for PSD import

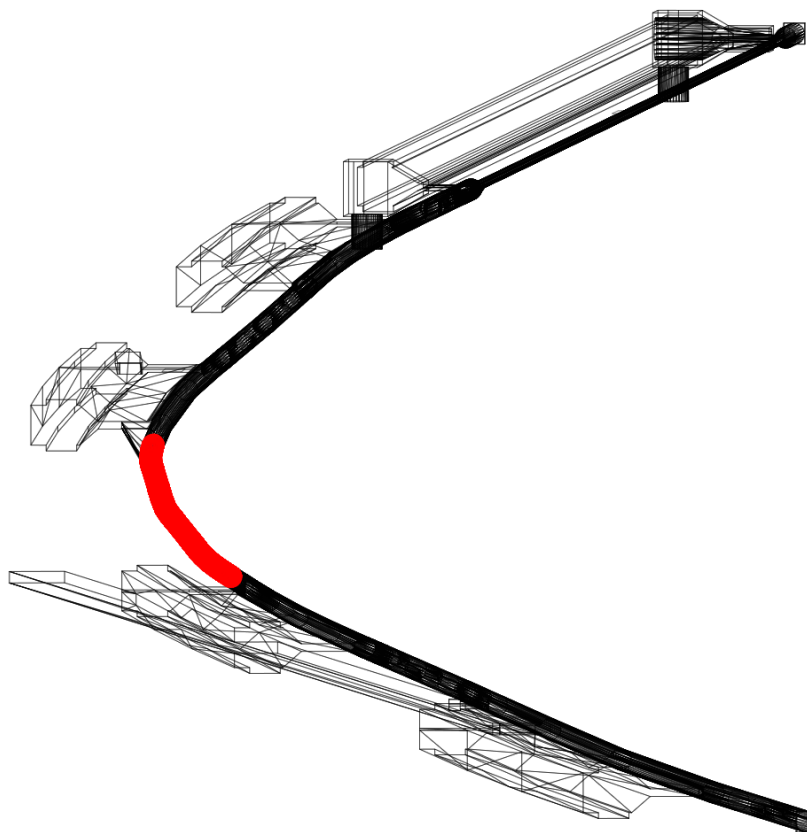


Figure 6.1.3 NEG coated surfaces for PSD import

GAS	FOERSTER (APS) ALUMINUM (MBAR*L/S)	GROBNER (LEP) (MBAR*L/S)	MATHEWSON (ELLIPSE) (MBAR*L/S)	KOBARI (NSLS) (MBAR*L/S)
H₂	6.76E-7	1.23E-5	2.07E-6	2.98E-6
CO ₂	8.45E-8	7.73E-7	4.52E-7	2.65E-7
CO	9.94E-8	5.18E-7	1.67E-7	8.91E-7
CH ₄	1.46E-8	1.25E-8	1.20E-8	1.62E-8
TOTAL	8.75E-7	1.36E-5	2.71E-6	4.15E-6

Table 6.1.1 Comparison of total outgassing @ 1000 A*hrs using four separate aluminum PSD measurements

6.2. MolFlow+ results

Figure 6.2.1 and Figure 6.2.2 feature pressure profiles for the four major vacuum gases computed along the center of the beam path for 100 A*hrs. and 1000 A*hrs. beam conditioning time. These pressure profiles were computed using Kobari's PSD measurement from the NSLS aluminum extrusion. Figure 6.2.3 compares the total pressures @ 1000 A*hrs beam conditioning using four separate aluminum PSD measurements.

Table 6.2.1 shows the pressure profiles using four separate aluminum PSD measurements. Table 6.2.2 compares the average gas compositions using four separate aluminum PSD measurements.

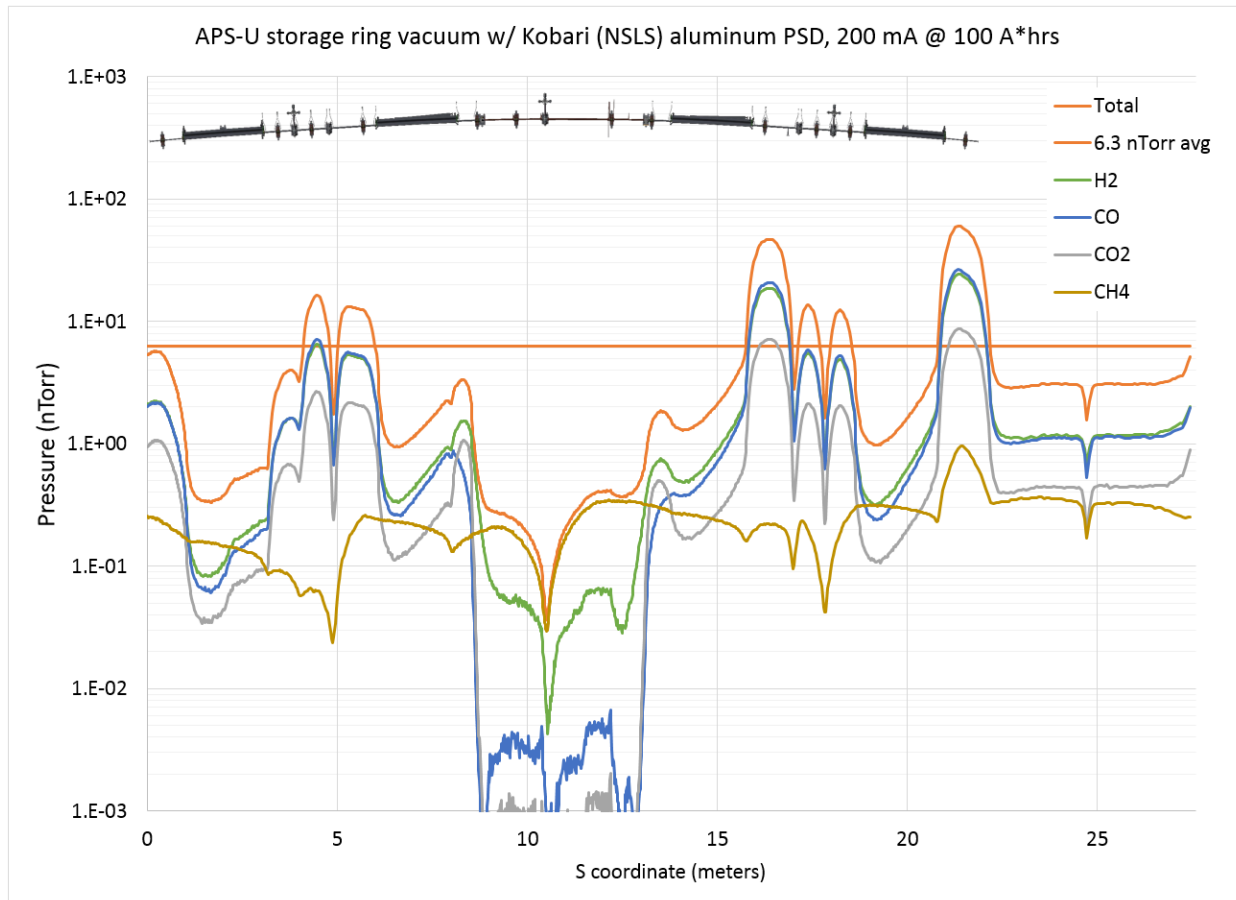


Figure 6.2.1 Gas specific MolFlow+ pressure profiles @ 100 A*hrs. beam conditioning for a simulation using the Kobari (NSLS) aluminum PSD measurement

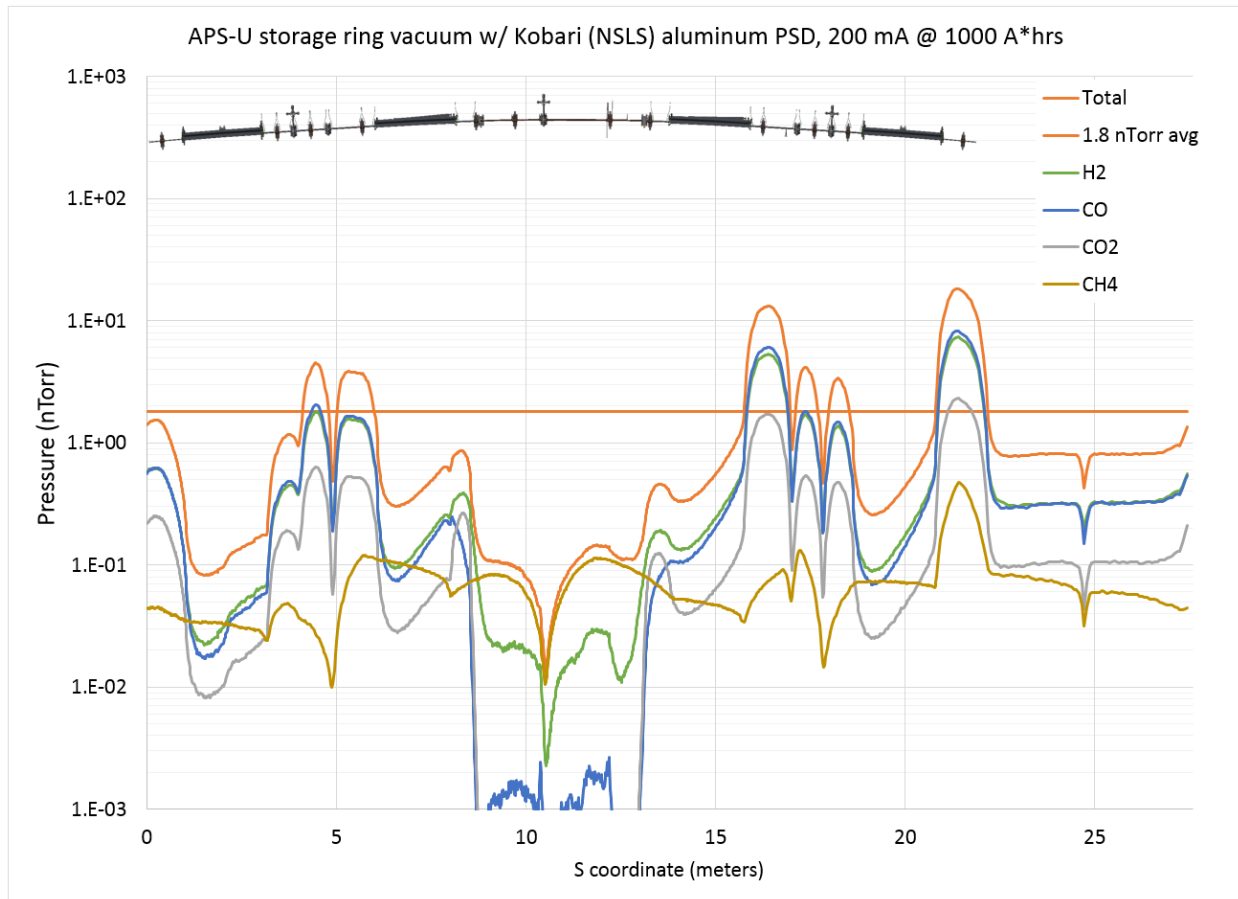


Figure 6.2.2 Gas specific MolFlow+ pressure profiles @ 1000 A*hrs. beam conditioning for a simulation using the Kobari (NSLS) aluminum PSD measurement

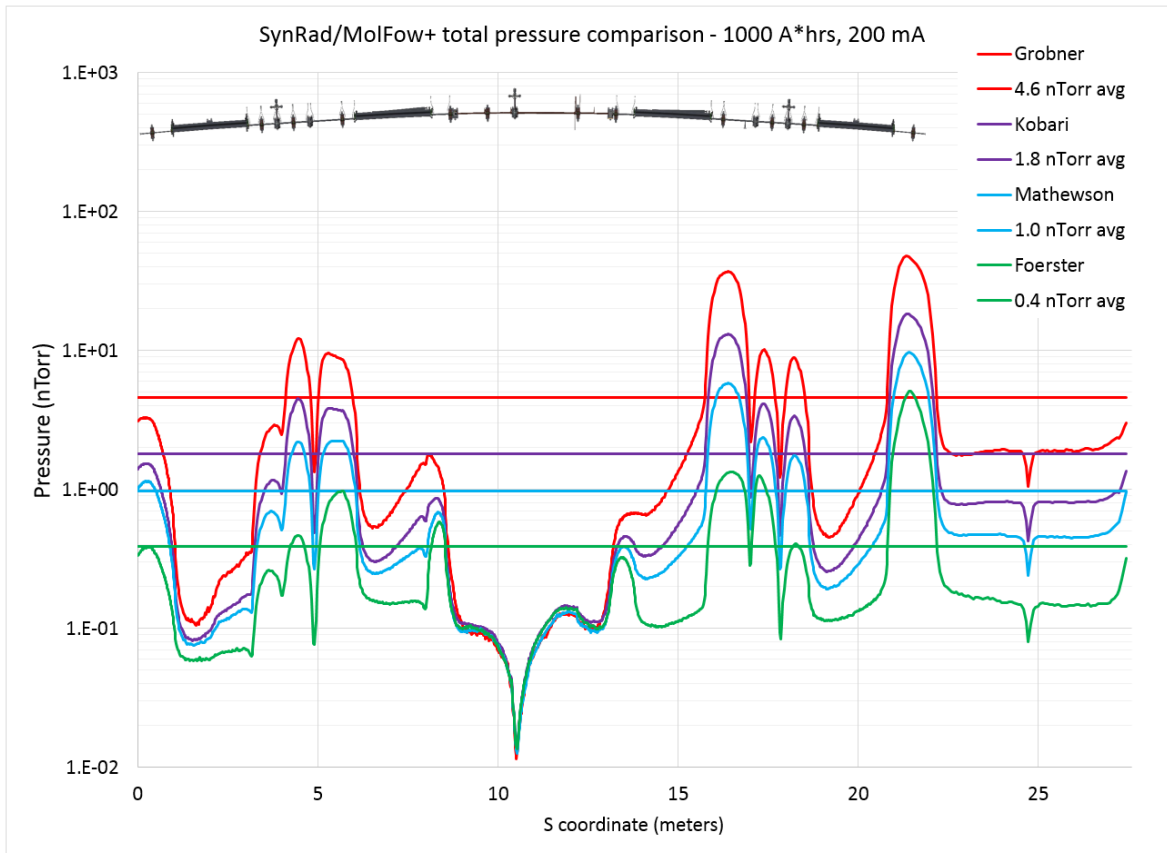


Figure 6.2.3 Total pressure comparison @ 1000 A*hrs using four separate aluminum PSD measurements

GAS	FOERSTER (APS) (NTORR)	GROBNER (LEP) (NTORR)	MATHEWSON (ELLIPSE) (NTORR)	KOBARI (NSLS) (NTORR)
H ₂	0.16	3.13	0.43	0.72
CO ₂	0.07	0.87	0.35	0.23
CO	0.10	0.51	0.13	0.76
CH ₄	0.07	0.06	0.05	0.07
TOTAL	0.39	4.57	0.97	1.79

Table 6.2.1 Comparison of total pressure @ 1000 A*hrs conditioning using four separate aluminum PSD measurements

GAS	FOERSTER (APS)	GROBNER (LEP)	MATHEWSON (ELLIPSE)	KOBARI (NSLS)
H ₂	40%	68%	45%	40%
CO ₂	17%)	19%	36%	13%
CO	25%	11%	14%	43%
CH ₄	17%	1%	5%	4%

Table 6.2.2 Comparison of average gas compositions @ 1000 A*hrs conditioning using four separate aluminum PSD measurements

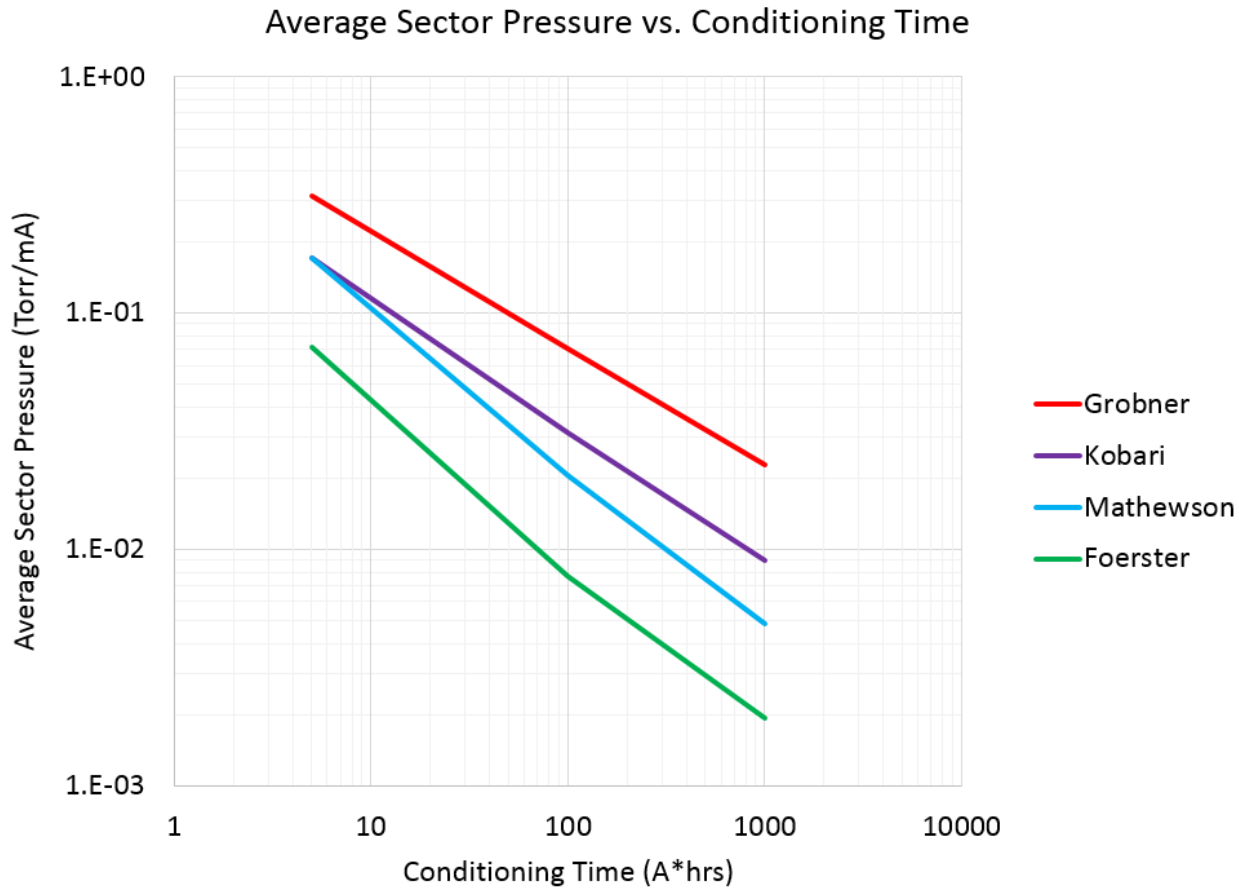


Figure 6.2.4 Comparison of APS-U conditioning curves for four aluminum PSD measurements

6.2.1. NEG saturation/failure analysis

Both NEG coatings and NEG pumps saturate with increased desorption as shown in the pumping curves in Section 3. Approximating the degree of saturation is difficult in a complex system with varying levels of desorption so separate SynRad/MolFlow analyses are compared in Figure 6.2.5 with conservative assumptions of full pumping saturation for the various NEG elements. For saturated NEG coatings, recent PSD measurements have shown that NEG coatings maintain low PSD levels even when their pumping is not activated [23] so results from this PSD measurement will be used in cases where the NEG coatings are assumed saturated.

The three scenarios for comparison are:

1. Saturated NEG coatings in the FODO section (no pumping but still low non-activated NEG coating PSD levels applied to FODO section surfaces)
2. Burnt NEG coatings in the FODO section (no pumping, copper PSD levels along the primary photon stripe, non-activated NEG PSD levels on remaining FODO surfaces). This assumes a scenario where synchrotron radiation burns off the coating along the primary photon stripe.

3. Saturated NEG coatings, NEG strips and CapaciTorr throughout the sector. This is the most conservative pumping scenario where the only pumping remaining is from ion pumps.

The results show that scenarios 1 and 2 are not debilitating with only a 30% pressure rise if the NEG coating was ‘burnt’ to the copper below. Scenario 3 contains seemingly very rare scenarios where many of these elements can be recharged or replaced if detected.

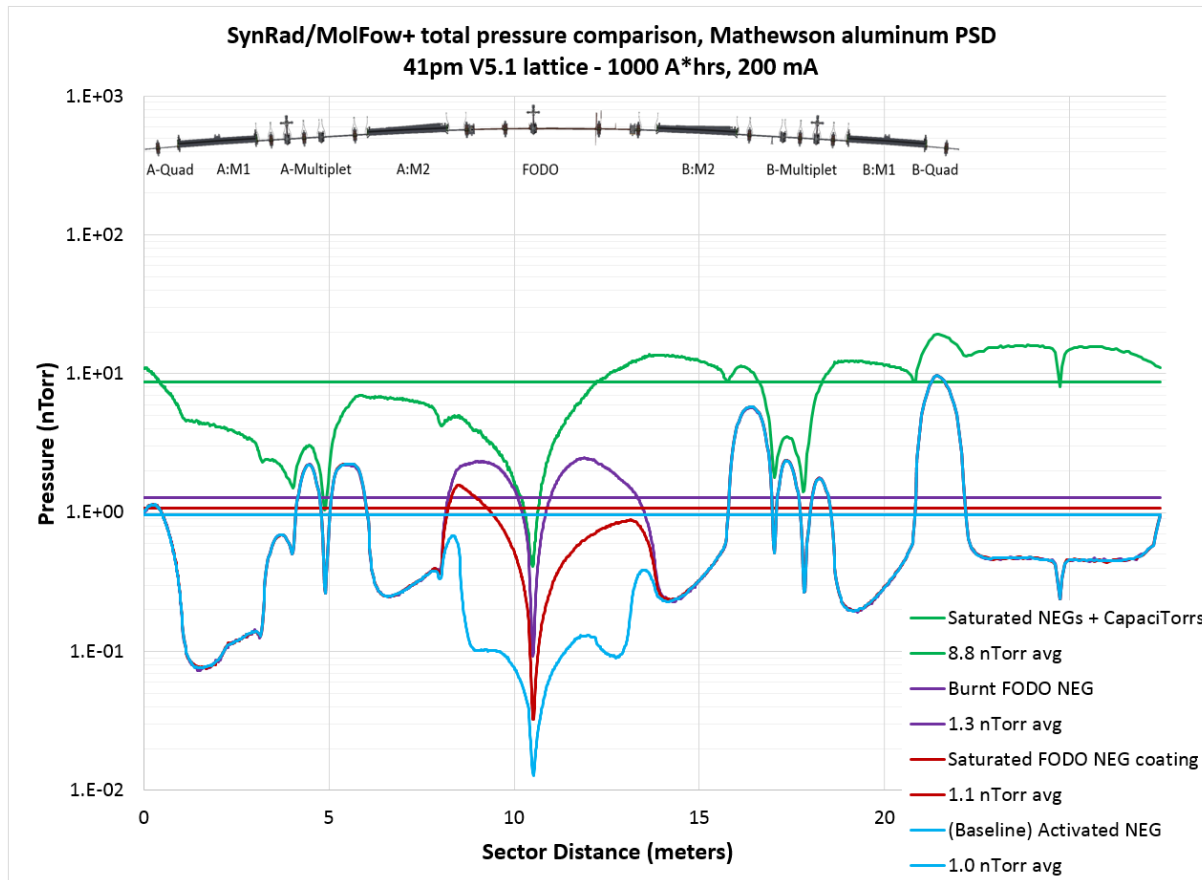


Figure 6.2.5 Comparison of APS-U pressures for various NEG saturation or failure scenarios

6.3. Comments on results

The total average pressure across a sector with the Kobari NSLS aluminum PSD measurement, see Table 6.2.1, Table 6.2.2, Figure 6.2.1, and Figure 6.2.2, is computed to be 6.3 nTorr at 100 A*hrs. beam conditioning and 1.8 nTorr at 1000 A*hrs. The gas specific average pressures are highest for H₂, however the heavier gases such as CO and CO₂ have the most influence on beam lifetime and they are of higher priority to address.

The high-pressure bumps occur in regions that have primary photon incidence, are not NEG coated, and have no distributed pumping or exist between two pumping elements. The high-pressure bumps occur primarily in the A and B multiplet chambers and the BQ7. The high outgassing in these chambers occur at absorbers where primary photons collect in high concentrations and at more diffuse secondary photon ‘hot

spots' where the photons collect after scattering off of the absorbers. These chambers also have poor pumping conductance due to their narrow apertures over long lengths. Figure 6.2.1 and Figure 6.2.2 show that the high pressure bumps define the average pressure values.

Low pressures occur at discrete pump locations and in regions that are NEG coated or have distributed pumping such as the four L-bend chambers, the FODO section, and the straight section. Distributed pumping makes poor pumping conductance of a narrow chamber a much less significant factor. The FODO section has very low pressures specifically for the gases CO, CO₂, and H₂O due to the combined effect of low PSD gas yields and high pumping speeds for these gases that are inherent to the NEG coating.

The pressure profiles for CH₄ (methane) have shapes unique to the other gases as the NEG coating and NEG strips are assumed to not provide CH₄ pumping. The MolFlow+ simulations predict that CH₄ pressures would dominate in the NEG coated FODO section.

6.3.1. Comments on aluminum PSD measurement study

Figure 6.2.3 shows four pressure profiles calculated with four separate PSD measurements as inputs. The four profiles are very similar in profile but their magnitude varies with a range of averages from 0.39 nTorr to 4.57 nTorr. The variation between the four pressure profiles reveals the importance of considering numerous sources of experimental data in order to anticipate the error bars possible for the analysis. Understanding the behavior of irradiated aluminum surfaces is key for this analysis as they represent ~90% of the outgassing surface area in the model. The results indicate that unfortunately one PSD measurement will not reveal a unique behavior for a given material such as aluminum but that the results may vary based on a number of factors related to the chamber design and bakeout conditions as discussed in Section 4.2.1.

Fortunately, the highest average pressure predicted using the Grobner measurement is the only result above the 2 nTorr design target and is not far from it. The results from this study indicate that a new PSD measurement could help build confidence in the pressure predictions of the APS-U storage ring vacuum system if taken from an aluminum chamber produced and cleaned under conditions equal or very similar to that of future APS-U aluminum vacuum chamber designs.

References

- [1] R. Kersevan and M. Ady, "MolFlow+ - A Monte-Carlo Simulator Package developed at CERN," CERN VSC Group, 2015. [Online]. Available: <http://test-molflow.web.cern.ch/>.
- [2] "41pm V5.1 lattice summary files for PDR, APS-U Sharepoint," 2017. [Online]. Available: https://icmsdocs.aps.anl.gov/docs/idcplg?IdcService=DISPLAY_URL&dDocName=APSU_1705315.
- [3] B. Stillwell, "41pm V5.1 Ray Trace Layout," 2017. [Online]. Available: https://apsshare.aps.anl.gov/apsu/MBAWorkingGroup/Shared%20Documents/Vacuum/Drawings%20-%20Top-Level%20Layouts%20and%20Ray%20Traces/MBA_VAC_MAG_RAY_TRACES_41PM_V5.pdf.
- [4] G. Decker and M. Borland, "APS MBA Accelerator Systems Functional Requirements," October 2014. [Online]. Available: https://apsshare.aps.anl.gov/apsu/MBAWorkingGroup/Shared%20Documents/Requirements%20and%20Parameters/APS-MBA-FReD_draft_28Oct2014.pdf.
- [5] "TiTan 45S Ion Pump Specification Sheet," [Online]. Available: <http://www.gammavacuum.com>.
- [6] "Perkin Elmer instruction manual - Ion pumps 60 L/s to 500 L/s," [Online]. Available: <http://www.perkinelmer.com>.
- [7] "SAES CapaciTorr MK5 Series Specification Sheet," 2015. [Online]. Available: <http://www.saesgetters.com>.
- [8] J. Moore, C. Davis and M. Coplan, Building Scientific Apparatus 2nd Edition, Cambridge UK: Cambridge University Press, 1989.
- [9] C. Liu and J. Noonan, "ANL/APS TB-16 - Advanced Photon Source Accelerator Ultrahigh Vacuum Guide," 1994. [Online]. Available: https://icmsdocs.aps.anl.gov/docs/groups/aps/documents/report/aps_1422143.pdf.
- [10] P. Chiggiato and P. C. Pinto, "Ti-Zr-V non-evaporable getter films: From development to large scale production for the Large Hadron Collider," *Thin Solid Films*, vol. 515, no. 2, pp. 382-388, 2003.
- [11] C. Benvenuti, P. Chiggiato, P. C. Pinto, A. Santana, T. Hedley, A. Mongelluzzo, V. Ruzinov and I. Wevers, "Vacuum properties of TiZrV non-evaporable getter films," *Vacuum*, vol. 60, no. 1-2, pp. 57-65, 2001.
- [12] R. Kersevan and M. Ady, *Private communications with Roberto Kersevan and Marton Ady of CERN VSCT group*, 2015.
- [13] C. Foerster, "Synchrotron light source measurements of photon stimulated desorption from vacuum chamber materials," *Synchrotron Radiation News*, vol. 11, no. 5, pp. 20-26, 1998.
- [14] P. Chiggiato and R. Kersevan, "Synchrotron radiation-induced desorption from a NEG-coated vacuum chamber," *Vacuum*, vol. 60, no. 1-2, pp. 67-72, 2001.
- [15] C. Foerster, C. Lanni, J. Noonan and R. Rosenberg, "Photon stimulated desorption measurement of an extruded aluminum beam chamber for the Advanced Photon Source," *Journal of Vacuum Science & Technology*, vol. A, no. 14, p. 1273, 1996.
- [16] O. Grobner, A. Mathewson, H. Stori and P. Strubin, "Studies of photon induced gas desorption using synchrotron radiation," *Vacuum*, vol. 33, no. 7, pp. 397-406, 1983.
- [17] T. Kobari and H. Halama, "Photon stimulated desorption from a vacuum chamber at the National Synchrotron Light Source," *Journal of Vacuum Science & Technology A*, vol. 5, no. 4, pp. 2355-2358, 1987.

- [18] A. Mathewson, O. Grobner, P. Strubin, P. Marin and R. Souchet, "Comparison of synchrotron radiation induced gas desorption from Al, stainless steel, and Cu chambers," CERN, 1990.
- [19] C. Foerster, C. Lanni, C. Perkins, M. Calderon and W. Barletta, "Photon stimulated desorption measurements of extruded copper and of welded copper beam chambers for the PEP-II asymmetric B factory," *Journal of Vacuum Science & Technology*, vol. A, no. 13, p. 581, 1995.
- [20] C. Foerster, H. Halama and C. Lanni, "Photon-stimulated desorption yields from stainless steel and copper-plated beam tubes with various pretreatments," *Journal of Vacuum Science & Technology*, vol. A, no. 8, p. 2856, 1990.
- [21] B. Henke, E. Gullikson and J. Davis, "X-Ray Interactions: Photoabsorption, Scattering, Transmission, and Reflection at $E=50 - 30,000$ eV, $Z = 1-92$," *Atomic Data and Nuclear Data Tables*, vol. 54, no. 2, pp. 181-342, 1993.
- [22] K. Harkay, *Private Communications with Kathy Harkay APS-XSD Physicist*, 2015.
- [23] M. Ady, P. Chiggiato, R. Kersevan, Y. Tanimoto and T. Honda, "Photodesorption and Electron Yield Measurements of Thin Film Coatings for Future Accelerators," in *IPAC2015*, Richmond, VA, 2015.